OPEN ACCESS

Review—Tetraruthenated Porphyrins and Composites as Catalysts and Sensor Materials: A Short Review

ECS Journal of Solid State Science and Technology, 2020 **9** 061011

Review—Tetraruthenated Porphyrins and Composites as Catalysts and Sensor Materials: A Short Review

Josué M. Gonçalves,[1] Tiago A. Matias,[1,2] Lucio Angnes,[1] Paulo R. Martins,[3] and Koiti Araki[1,z]

[1]*Department of Fundamental Chemistry, Institute of Chemistry, University of São Paulo, 05508-000, São Paulo, SP, Brazil*
[2]*Center for Natural and Human Sciences (CCNH), Federal University of ABC (UFABC), Santo Andre, SP, Brazil*
[3]*Institute of Chemistry Federal University of Goias, Goiania, GO 74690-900, Brazil*

Electrocatalytic and photocatalytic materials for energy and sensor applications are among the most relevant ones to overcome the challenges for a sustainable society. In this context, metalloporphyrins and transition metal complexes are known to exhibit interesting complimentary properties that can be combined to provide synergic effects, which was achieved in what so called tetraruthenated porphyrins and derivatives. The properties of these supramolecular species can be tuned based on the transition metal ion coordinated to the porphyrin, the ruthenium complex and especially the electronic coupling between those species conferring enhanced photoelectrochemical activity for conversion of carbon dioxide in valuable reduced species, or nitrite/nitrate to less harmful species. Another major application was shown to be as sensor materials for several substrates, generating more sensitive and robust devices. However, such a coordination chemistry strategy is evolving leading to new composite, polymeric and hybrids materials based on carbon nanomaterials, as well as 2D and 3D porous materials, opening new perspectives on supramolecular porphyrin chemistry powered by the versatile coordination chemistry of transition metal ions and clusters. This short review revisits the interesting spectroelectrochemistry and applications of tetraruthenated porphyrins, expanding to the most recent works pointing towards auspicious new outcomes in near future.

 [DOI: 10.1149/2162-8777/aba4f5]

Manuscript submitted May 30, 2020; revised manuscript received July 8, 2020. Published July 20, 2020. *This paper is part of the JSS Focus Issue on Porphyrins, Phthalocyanines, and Supramolecular Assemblies in Honor of Karl M. Kadish.*

Biological systems have inspired the development of science by providing examples of sophisticated molecular based machines and systems yet not explored or understood. Supramolecular chemistry is all about the combination of molecular species in more complex systems exploiting the additive and synergic effects to generate new functionalities.[1] The assembly of the molecular entities should be carried out in an organized way through covalent bonds, electrostatic forces and/or weak van der Waals interactions. In this way, it is possible to devise an infinite number of possibilities exploiting the chemistry of already known species. Among the possibilities, the coordination chemistry approach provides a unique and rather attractive approach since the several structural features and versatility of the metal–ligand bonds and interactions are fully available to build more complex architectures, concomitantly with the incorporation of catalytic, electrochemically, photochemically active and magnetic sites in the material. In addition, the electronic coupling with the other components, or in other words the functionalities, can be tuned by the bridging species while incorporating molecular recognition and self-assembly properties. In fact, Lehn[2] regarded supramolecular chemistry as a generalization of coordination chemistry[1] because of the intrinsic similarities of assembling strategies based on weaker interactions.

The supramolecular assembly approach based on coordination chemistry is primarily directed by the metal–ligand affinities, stereochemistry and substitution properties of metal ion sites.[1] Thus, the metallic element and its oxidation state, as well as the ligand type, can be chosen in order to favor the interactions and assemble newly designed systems by combining molecular unities with complementary properties to achieve a desired functionality. In this context, photochemically and electrochemically active donor/acceptor groups based on transition metal complexes and nanomaterials such as porphyrins, and related macrocycles, and ruthenium polypyridyl complexes can be put together with polyoxometalate clusters, as well as oxides and metallic nanoparticles, to build photoelectrocatalytically active materials with enhanced electrochemical/electrocatalytic and charge-transfer/charge storage/charge separation properties.[1,3] As consequence, the coordination chemistry approach is a versatile strategy to build functional supramolecular systems and hybrid nanomaterials.

Porphyrins are present in nature in more systems than we are generally aware of and their existence is known for more than a century. In biological systems, the presence of these compounds and their derivatives are ubiquitous, being the active center in hemoglobin and myoglobin of humans and animals. These macrocyclic compounds are present in the cytochrome P-450 enzyme of several organisms, from humans to microbial organisms.[4] They are also found in non-living sites, being named as petroporphyrins when found in crude oil, oil shale[5] or geoporphyrins when found in rocks and coal.[6] Finally, metalloporphyrins are the active site in the structure of enzymes catalyzing an extremely wide range of redox reactions and are fundamental in many detoxification reactions.

The area of synthetic porphyrins started long ago with Rothemund[7] is continuously evolving since since new and more efficient routes for preparation of many different porphyrins were developed[8–10] increasing the possibilities for synthesis of macrocycles with increasing complexity. Their unique properties can be explored for many different perspectives and applications, such that porphyrins and related macrocycles chemistry is one of the most active field in chemistry, as can be seen in the literature and in the 20 volumes of "The Handbook of Porphyrin Science".[11] This comprehensive series describes the synthetic routes, as well as the main properties and applications such as spectroscopic, electrochemical, crystallographic, non-linear optics, photochemical and photodynamic therapy, as well as other applications in biomedical areas.

Recently the heterocomponents of ternary supramolecular complexes of porphyrins have been summarized by Prigorchenko et al.[12] In short, they reviewed the non-covalently bound ternary complexes of porphyrins, assembled from at least three non-identical species and highlighted a collection of sophisticated molecular architectures including sandwich-type complexes, cages, capsules, tweezers, rotaxanes, and other supramolecular architectures mediating oxygen-binding and oxidation reactions. Additionally, Percásteguia & Jancikab[13] provided an overview of the recent advances in the

[z]E-mail: koiaraki@iq.usp.br

field of discrete metal–ligand assemblies based on *meso*-substituted metallo-porphyrins, with a particular focus on the new functionalities that emerge from self-assembly and framed the perspectives for future areas of research. First, they described notable examples of metallo-porphyrins functionalized with coordinating groups, which have served as building blocks to create discrete porous "Coordination Cages", followed by the progress in the synthesis of *meso*-substituted metallo-porphyrins and provided new methodological insights for the design of coordination-based porphyrin assemblies, enhancing their properties and allowing the rise of new functions.

More specifically, Toma & Araki (2000)[1] reviewed a notable series of porphyrins and ruthenium complexes, systematically investigated from 1990 to 2000. Matias and colleagues[3] in their book chapter reviewed the well-defined and well-characterized supramolecular systems constituted by porphyrins and peripheral electrochemically and photochemically active transition metal complexes, dendrimers made of porphyrins and phthalocyanines, as well as nanostructured interfaces and hybrid nanomaterials obtained by binding metal and metal oxide nanocrystals, and carbon-based nanoparticles to those macrocycles. However, in this broad context, a little attention was paid to Tetra-Ruthenated Porphyrins, TRPs, *meso*-substituted porphyrins with four ruthenium complexes bound to the macrocyclic ring periphery.

In fact, there has been a growing interest in the application of TRPs and composites as catalysts and sensors in the last 10 years that deserve to be reviewed especially given their distinguished behavior in electrocatalysis and sensors. Accordingly, the main synthesis routes will be reported, as well as the application in chemically modified electrodes for electrocatalysis, photoelectrocatalysis and electrochemical sensors, highlighting the most relevant methods of immobilization of those molecular catalysts and the perspectives in this field.

Syntheses of Tetraruthenated porphyrins and spectroelectrochemical behavior

Porphyrins can be prepared by Adler-Longo[14] or Lindsey[15] method, the first one resulting in moderate yields (about 10%–20%) by refluxing equimolar amounts of pyrrole and aryl-aldehyde in propionic or acetic acid. The Lindsey method involve two steps, the reaction of aryl-aldehydes and pyrrole in diluted CH_2Cl_2 solution, in presence of a Lewis acid catalyst such as boron trifluoride diethyl etherate or trifluoroacetic acid. The porphyrinogen generated in this step is oxidized to porphyrin using a quinone such as 2,3-dichloro-5,6-dicyanobenzoquinone (DDQ) as oxidant in a second step, in good yields (about 30%–40%). The use of a single type of aldehyde generates the corresponding 5,10,15,20-tetraarylporphyrin or *meso*-tetraarylporphyrin. It is also possible to prepare tetraarylporphyrins substituted with more than one type of aryl groups by using distinct aldehydes and controlling their relative molar ratios. However, these result in low yields of the desired molecules due to the formation of a mixture of products.

The use of 4-pyridinecarboxaldehyde, or its isomers, produces the *meso*-tetra(4-pyridyl)porphyrin (H_2(4-TPyP), see Fig. 1), a molecule having perimetral pyridyl N-atoms sites enabling the coordination of transition metal complexes. This approach was shown to be interesting for the development of supramolecular electrocatalysts since the peripheral transition metal complexes have strong enough electronic coupling with the macrocycle to influence its electronic, redox and catalytic properties, particularly for multi-electron redox processes.[3]

The preparation of tetraruthenated porphyrins H_2(TRuP) is performed by the reaction de H_2(TPyP) with complexes such as $[RuCl(H_2O)(bpy)_2]^{2+}$ (bpy = 2,2′-bipyridine). For an efficient reaction, the porphyrin and complex should be solubilized in a same solvent. One of the earliest success was achieved by the reaction of H_2(4-TPyP) with $[RuCl_2(bpy)_2]$ (1:4.1 molar ratio) in refluxing glacial acetic acid for 45 min. In this first stage, mono, bi or triruthenated porphyrin species probably are formed. To generate the desired TRuP, the solvent was removed in a flash evaporator, the solid redissolved in a minimum volume of methanol and refluxed for 45 min.[16] The supramolecular species is soluble in most organic solvents and can be metallated by reaction of TRuP with transition metal ions salts. It is also possible to synthesize [M(TRuP)] directly by reaction of [M(4-TPyP)] with $[RuCl_2(bpy)_2]$.[17] In some cases hydrochloric acid can be used to solubilize TPyP in methanol, then the reaction with $[RuCl_2(Clphen)_2]$ (Clphen = 5-Chloro-1,10-phenanthroline) was performed in a mixture of methanol:DMF (1:4 v/v) as solvent.[18] Furthermore the employment of 2,2,2-trifluoroethanol (TFE) as a solvent has enabled the direct reaction of TPyP with most metal complexes.[19] Indeed, TFE is a very useful solvent for synthetic chemistry purposes since possesses an interesting set of properties. One of most interesting among them is the capability to solubilize many organic and inorganic compounds thus been a suitable medium for preparation of supramolecular species. In other cases, the ruthenium complex is soluble in organic solvents such as $CHCl_3$ and CH_2Cl_2 and the reaction between the porphyrin and the transition metal compound can be carried out in these solvents.[20] The structures of porphyrins and some complexes used to generate supramolecular species are shown in Fig. 1.

The UV–Vis spectra of TRuP has contributions from the porphyrin and the ruthenium complex. The H_2(3-TPyP) and H_2(4-TPyP) species exhibited the Soret, $Q_{y(1-0)}$, $Q_{y(0-0)}$, $Q_{x(1-0)}$ and $Q_{x(0-0)}$ bands at 413, 512, 545, 587 and 646 nm, respectively, in chloroform,[21] whereas the absorption bands of porphyrin and tetraruthenated species are listed in Table I. The coordination of $[RuCl(bpy)_2]^+$ moieties to the pyridyl groups of those porphyrins yields H_2(3-TRuP) and H_2(4-TRuP) inducing a small perturbation to the respective pyridylporphyrin spectrum. The UV–Vis spectra of these species in methanol exhibited the porphyrin Soret, $Q_{y(1-0)}$, $Q_{y(0-0)}$, $Q_{x(1-0)}$ and $Q_{x(0-0)}$ bands at 417, 513, 547, 588 and 650 nm, and 416, 513, 554, 590 and 648 nm, respectively. Moreover, three new absorption bands was observed at 294, 360 and 480 nm, assigned to the 2,2′-bipyridine intraligand $p\pi \rightarrow p\pi^*$ and two $Ru^{II}(d\pi) \rightarrow bpy(p\pi^*)$ charge-transfer transitions, respectively.[16,21] Interestingly, molecular modeling calculations showed that the electronic coupling of the ruthenium complexes and the porphyrin ring is dependent on the pyridyl bridge dihedral angle and can be insignificant when it is orthogonal to the macrocyclic ring. Generally, the angle was lower for the *para*-isomer in comparison with the *meta*-isomer, as expected for a lower steric hindrance between the *ortho*-pyridyl and ß-pyrrole H-atoms caused by a saddle distortion of the porphyrin ring.[21] As a result, the HOMO of H_2(4-TRuP) species is predominantly localized on the ruthenium polypyridyl complexes (66%), with a substantial contribution from the porphyrin moiety (24%), where the electronic density is concentrated on the pyrrole nitrogen and *meso*-carbon atoms. The LUMO are formed by two orbitals highly localized on the porphyrin ring (≈90%). The bridging pyridyl groups contribute with about 10% for the HOMO and LUMO composition, favoring the electronic coupling of the porphyrin with the peripheral ruthenium complexes in the ground and excited states.[21] In contrast, the HOMO of the H_2(3-TRuP) species comes out to be essentially localized (89%) on the ruthenium complexes and the pyridyl bridging groups (9%), while the contribution of the porphyrin ring is very small (<2%).

On the other hand, the two lowest energy LUMOs are essentially localized on the porphyrin ring (91%) and on the pyridyl-bridging group (9%), in analogy with the *para*-isomer.[21] The protonation of both free-base porphyrin rings generates the H_4(3-TRuP) and H_4(4-TRuP) species, where the first isomer exhibited a spectrum resembling the sum of the ruthenium complex and the protonated-porphyrin absorption bands. In contrast, in addition to the bpy intraligand $p\pi \rightarrow p\pi^*$ at 294 nm and the Soret band at 443 nm, the spectrum of the H_4(4-TRuP) species exhibited two broad features at 560 and 704 nm in acidified methanol solution, instead of the typical porphyrin spectral profile with two sharp bands in the visible range. The lowest energy absorption band was assigned to a $Ru^{II}(d\pi) \rightarrow$

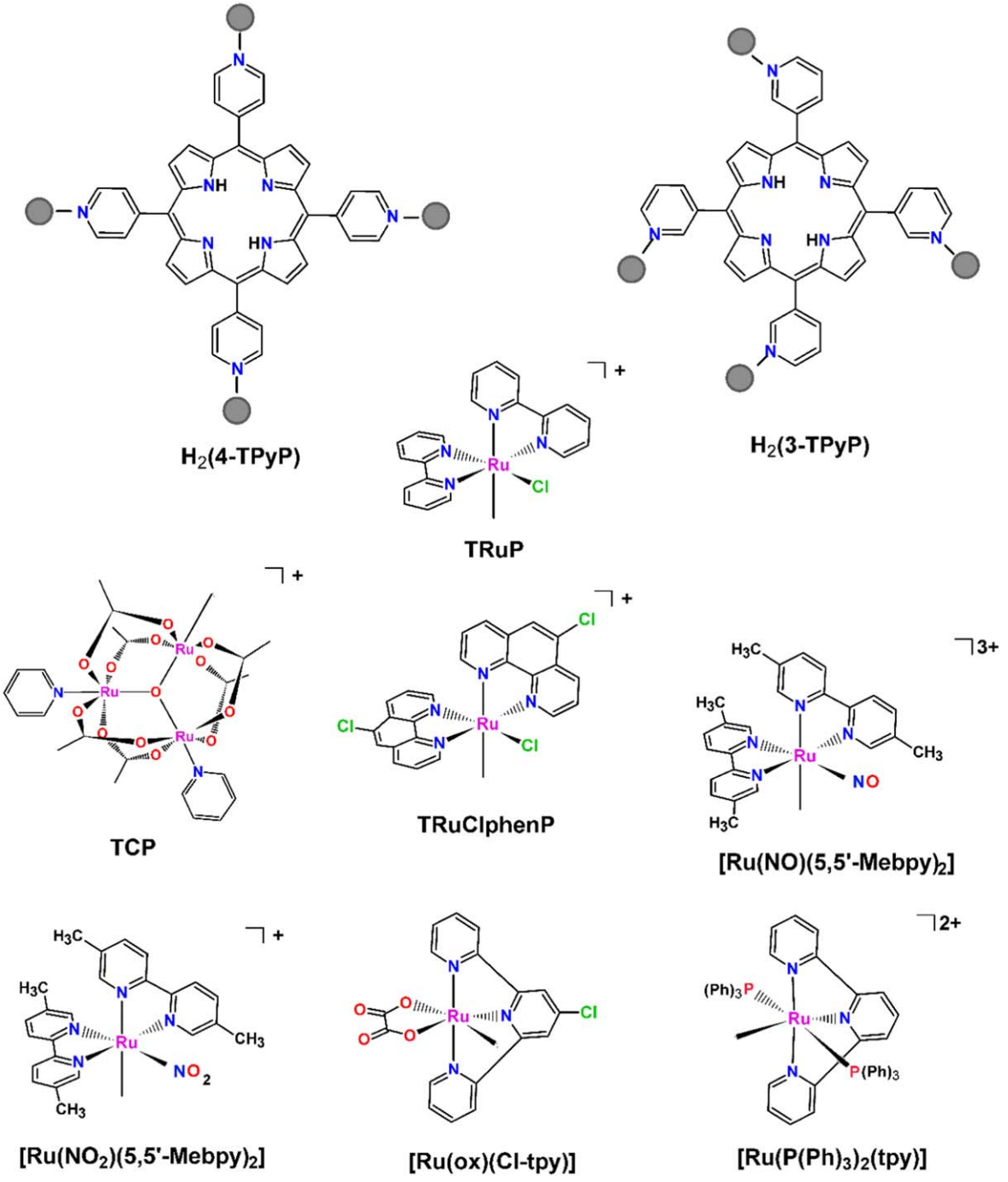

Figure 1. Structure of meso-substituted porphyrins and tetraruthenated porphyrins. The gray spheres represent the peripheral coordination complexes depicted below them.

H_4(4-TPyP) charge-transfer transition. The porphyrin π orbitals are stabilized by the bis-protonation of the ring, consequently increasing the contribution of porphyrin orbitals in the HOMO.[16,21] Similar behavior was exhibited respectively by H_2(3-TCP) and H_2(4-TCP) where the porphyrin pyridyl groups are coordinated to four $[Ru_3O(CH_3CO_2)_6(py)_2]$ complexes. The Soret and Q bands of these species are almost identical to that of H_2(TRuP), showing a small perturbation of the H_2(TPyP) electronic structure,[22] see Table I. It was also possible to observe the characteristic transitions of the cluster units, the py $p\pi \rightarrow p\pi^*$ bands at 235 and 274 nm for both, the isomers substituted in the 3- and 4-positions, whilst the four bands at 419, 515, 550, 645 and 702 nm and 418, 515, 550, 645 and 706 nm were respectively assigned to the H_2(3-TCP) and H_2(4-TCP) porphyrin π-π^* and intracluster (IC) transitions.[22] The cluster-to-ligand charge transfer (CLCT) $Ru_3O \rightarrow p\pi^*$ (py ligand of cluster) bands of both isomers arise at 317 nm. Noteworthy was the new band at 355 nm assigned to the charge transfer from Ru_3O unit to the bridging pyridyl–porphyrin groups. The spectrum of H_4(4-TCP) resembles that of H_4(4-TRuP) species showing the cluster-to-porphyrin charge transfer transition at 720 nm.[22]

The coordination of $[RuCl(Clphen)_2]^+$ to H_2(TPyP) generated (Fig. 1) H_2(4-TRuClphenP), whose UV–vis spectrum in methanol exhibited, as expected, the characteristic peaks of the free-base porphyrin at 419 nm, 513 ($Q_{y(0-1)}$), 552 ($Q_{y(0-0)}$), 588 ($Q_{x(0-1)}$), and 648 nm ($Q_{x(0-0)}$) without significant electronic disturbance induced by the peripheral ruthenium complexes. On the other hand, the

Table I. Absorption bands of tetraruthenated porphyrin species.

Compounds	Porphyrin moiety (nm)	Peripheral complexes (nm)	References
H_2(3-TPyP)[a]	413, 512, 545, 587, 646[a]	—	21
H_2(4-TPyP)	413, 512, 545, 587, 646	—	21
H_2(3-TRuP)	417, 513, 547, 588, 650[b]	294, 360, 480	21
H_2(4-TRuP)	416, 513, 554, 590, 648	294, 360, 480	16
H_2(3-TCP)	419, 515, 550, 589, 645	235, 312, 355, 420, 510, 615, 702	22
H_2(4-TCP)	418, 515, 552, 591, 652	235, 312, 355, 438, 508, 604, 706	22
H_2(4-RuClphenP)	419, 513, 552, 588, 648	295, 450	18
H_2(4-TRuoxP)	414, 514, 557, 588, 643	238, 311, 367, 449, 643	23
[Zn(3-TRuP)]	429, 560, 599	297, 370, 485	24
[Zn(4-TRuP)]	430, 562, 606	298, 358, 450–490	17
[Ni(4-TRuP)]	414, 530, 580	298, 354, 490,	25
[Co(4-TRuP)]	434, 546, 594	298, 356, 490	26
[Fe(4-TRuP)]	416, 568, 616	298, 362, 490	27
H_2(TPyViP)	369,417, 512, 546, 587, 643	—	28
H_2(TRuPyViP)	416, 512, 555, 592, 647	294, 485	28
[Zn(TRuPyViP)	427, 560, 602	293, 497	28
[Zn(4-TCP)]	436, 572, 619	324, 685	19
[Co(4-TCP)]	435, 557, 611	318, 693	29
[Mn(4-TCP)]	475, 584, 621	320, 694	30

absorption band of ruthenium complexes were impacted by the change of coordinated ligands. The intense and narrow band at 295 nm and the broad band at 450 nm are characteristic of the 5-Clphen $p\pi \rightarrow p\pi^*$ intraligand and $Ru^{II}(d\pi) \rightarrow$ Clphen($p\pi^*$) MLCT transitions, respectively.[18] The $[Ru(NO_2)(5,5'\text{-Mebpy})_2]^+$ and $[Ru(NO)(5,5'\text{-Mebpy})_2]^+$ groups (5,5′-Mebpy = 5,5′-dimethyl-2,2′-bipyridine, Fig. 1) have been recently coordinated to H_2(TPyP). As in H_2(4-TRuClphenP), the spectral profile of the new molecules was similar to the sum of porphyrin with ruthenium complexes absorption bands. However, the porphyrin spectrum is sufficiently intense to mask the metal-to-ligand charge transfer bands. The photochemical and photophysical properties of those porphyrins show that the complex containing nitrite is able to produce NO by homolytic O–NO bond cleavage.[31] In addition to bipyridine derivatives, terpyridine derivatives also can be used to generate tetraruthenated porphyrins. The $[Ru(H_2O)(ox)(Cl\text{-tpy})]$ (ox = oxalate ion, Cl-tpy = 4′-Chloro-2,2′:6′,2″-terpyridine, Fig. 1) complex was reacted with H_2(TPyP) in TFE to product H_2(4-TRuoxP).[23] The Soret band suffers a hypsochromic displacement of 5 nm after coordination with the peripheral complexes and appears at 414 nm. The bands at 514 nm, 557 nm and 588 nm were respectively assigned to the $Q_{y(0-1)}$, $Q_{y(0-0)}$ and $Q_{x(0-1)}$ transitions. In addition, the band at 643 nm can be assigned to a $Ru^{II}(d\pi) \rightarrow$ Cl-tpy ($p\pi^*$) MLCT transition, with strong overlapping of the $Q_{x(0-0)}$ transition. A second $Ru^{II}(d\pi) \rightarrow$ Cl-tpy($p\pi^*$) MLCT band at 449 nm, was more clearly observed after spectral deconvolution due to the overlapping with the vicinal Q bands. The band at 238 nm was attributed to a $p\pi \rightarrow p\pi^*$ transition of the polypyridyl ligand. The bands at 311 and 367 nm were assigned to $Ru^{II}(d\pi) \rightarrow$ (pyridyl-porphyrin) ($p\pi^*$) MLCT transitions. The HOMO of this species has predominantly contribution of ruthenium (50.81%), while the LUMO exhibits 99.93% contribution of porphyrin orbitals. The protonation of 4-TRuoxP porphyrin ring gives rise to a new band at 720 nm assigned to a Ru^{II} complexes-to-H_4(4-TRuoxPyP) charge-transfer transition. In the H_2(4-TRu(PPh_3)(tpy)P) species, where the peripheral complexes are *trans*-$[Ru(PPh_3)_2(tpy)]^{2+}$ (PPh_3 = triphenylphosphine, tpy = 2,2′:6′,2″-terpyridine, Fig. 1) the Soret band appears at 413 nm and the Q bands at 510, 545, 587 and 645 nm.[32] The absorption bands related to ruthenium complexes appear at 230, 268, 311, 334 and 470 nm, whilst the bands in the UV region has been ascribed to intraligand $p\pi \rightarrow p\pi^*$ transitions in both the terpyridine and the triphenylphosphine ligands. The lower energy absorption bands in the visible region were assigned to MLCT transitions having predominantly $Ru^{II}(d\pi) \rightarrow$ tpy($p\pi^*$) charge-transfer character. Interestingly, the steady state spectroscopy data suggested that the peripheral ruthenium groups mostly interact with the second excited singlet state orbitals of the porphyrin ring, while the lowest singlet excited state electronic properties are weakly perturbed.

The presence of the metal ion plays a dramatic effect on the properties of the metalloporphyrins. Metallated porphyrins typically have D_{4h} symmetry, and the two HOMO levels exhibit a_{2u} and a_{1u} symmetry while the LUMO level has e_g symmetry and is degenerate. The two electronic transitions arise from the a_{2u} and a_{1u} (HOMO) $\rightarrow$ (LUMO) e_g levels corresponding to the Soret and Q bands, respectively. The Q band is affected by a strong vibronic coupling, splitting it into two bands, namely Q_{0-0} and Q_{1-0}.[33] The [Zn(4-TRuP)] exhibits the characteristic Soret absorption band at 430 nm and the Q bands at 562 and 606 nm in DMF solution. The $[RuCl(bpy)_2]^+$ moieties absorption bands at 298, 358 and 450–-490 nm were respectively attributed to a $p\pi \rightarrow p\pi^*$ transition of bpy, and two MLCT $Ru^{II}(d\pi) \rightarrow$ bpy($p\pi^*$) transitions. The additional band at 466 nm was associated with the $Ru^{II}(d\pi) \rightarrow$ (pyridyl-porphyrin) ($p\pi^*$) MLCT transition.[17] The Soret band of the [Zn(3-TRuPyP)] isomer arises at 429 nm, the Q bands at 560 and 599 nm, the MLCT band at 485 and the ligand field band at 370 nm, while the $p\pi \rightarrow p\pi^*$ band of the bipy ligands is found at 297 nm in DMF solution.[24] In fact, in most metallated porphyrins, the ruthenium complexes absorption bands arise at 298 nm (bpy ligand) and around 356 and 490 nm (MLCT bands), showing less influence of the porphyrin moiety on the electronic structure of the $[RuCl(bpy)_2]^+$ peripheral complexes.[17] However, changes in the absorption band positions can be observed when electron withdrawing or donating groups are present in the bpy ligands, influencing the energy of the HOMO and LUMO orbitals of the peripheral complexes.[34,35] In the case of [M-(TRuP)] species with M = Cu(II), Ni(II), Co(II) and Fe (III), the Soret band arises in a very narrow range of the spectrum (415–416 nm), whereas the Q_{1-0} and Q_{0-0} bands can be found in the 530 to 568 nm and 580 to 618 nm range, respectively[17,24,25,27] (see Table I). The characteristic porphyrin bands of [M(4-TCP)], where M = Zn(II), Co(II), Mn(II), can be found in similar ranges of the spectrum. The Soret band in the 414–425 nm range for the Zn(II), Co(II) and Mn(II) complexes, but in the Mn(III) species appears around 475 nm, while the Q_{1-0} and Q_{0-0} bands can be respectively found in the 557–584 and 611–645 nm range. The characteristic intracluster band of the peripheral complexes was observed in the

685–707 nm range, whilst the $Ru^{III}_3O \rightarrow py$ ($p\pi^*$) MLCT band can be found in the 314–351 nm range.[19,22,29,30]

The tetraruthenated porphyrins exhibit a very rich electrochemistry associated with the redox processes localized in the porphyrin ring and the peripheral ruthenium complexes. In fact, up to seven redox processes can normally be observed in anhydrous solvents such as acetonitrile and dimethylformamide depending on the structure of the ruthenium complex.[22] The electrochemical data are consistent with the UV–vis absorption spectroscopy, indicating that the HOMO of H_2(TRuP) is located in the peripheral complexes and is modulated by the ligands coordinated to the ruthenium ion.[34,35] Thus, typically, it is possible to observe the oxidation process of the metal center to Ru(III) and two reductions process of the coordinated ligands. In contrast, the LUMO is centered on the porphyrin ring which can be reduced to the $H_2(TPyP)^-$ and $H_2(TPyP)^{2-}$ species in two consecutive monoelectronic processes. The macrocycle can also be oxidized by monoelectronic or bielectronic processes leading to the formation of the respective radical cation or dication species.[17,24,25,27] Metallated TRuP may exhibit additional redox processes localized on the metal ion, as shown in Table II, where the redox potentials of supramolecular H_2(TRuP) and [M(TRuP)] species are listed. The electrochemical behavior of H_2(TCP) and [M(TCP)] species is dominated by waves associated with the Ru_3O triruthenium cluster center since the II,II,III/II,III,III/III,III,III /III, III,IV/III,IV,IV redox species can be accessed,[19,22,29,30] as summarized in Table III.

More recently, other pyridyl porphyrins have also been used to generate tetraruthenated porphyrins. The free-base *meso*-tetra(4-pyridylvinylphenyl)porphyrin H_2(TPyViP) (see Fig. 2) exhibits the Soret band at 417 nm and the Q bands at 512, 546, 587 and 643 nm in acetonitrile solution, and the $p\pi$-$p\pi^*$ absorption band of the pyridyl-vinyl moiety at 369 nm. The tetraruthenated porphyrin H_2(TRuPyViP) prepared by conjugation of $[RuCl(bpy)_2]^+$ groups to the ring periphery exhibited absorption bands at 416 nm (Soret), 512 nm ($Q_{y(0-1)}$), 555 nm ($Q_{y(0-0)}$), 592 nm ($Q_{x(0-1)}$) and 647 nm ($Q_{x(0-0)}$), characteristic of the macrocyclic ring, while the typical 2,2′-bipyridine intraligand $p\pi \rightarrow p\pi^*$ and the two $Ru^{II}(d\pi) \rightarrow$ bpy ($p\pi^*$) charge-transfer transitions were found at 294 nm and 470–-490 nm range, respectively. The coordination of Zn(II) to the tetraruthenated porphyrin shifted the Soret band to 427 nm and the Q bands to 560 and 602 nm. The TRuPyViP shows three reversible redox processes in DMF solution. The wave at $E_{1/2} = +0.90$ V was assigned to the Ru(III/II) process, while the waves at −0.70 and −1.05 V were assigned to the first and second mono-electronic reduction processes of the porphyrin ring. The redox process associated with the ruthenium center (+0.89 V) is not significantly affected by the coordination of Zn(II) generating the Zn-TRuPyViP species, whilst the porphyrin ring reduction processes are shifted respectively to −0.99 and −1.21 V, and the ring oxidation process to +1.43 V.[28]

Another very interesting example are the supramolecular species assembled by coordination of $[RuCl(5,5'\text{-Mebpy})(dppb)]^+$ (dppb = 1,4-bis(diphenylphosphino)butane) complexes to *meso*-tetra(2-thienyl)-porphyrins (TThP) and *meso*-tetra(5-methyl-2-thienyl)-porphyrins (TMeThP) (Fig. 2).[36] Remarkable spectroelectrochemical behavior was found as compared with the 4-TPyP derivatives. The electronic spectrum of $\{[RuCl(5,5'\text{-Mebpy})(dppb)]_4(4\text{-TPyP})\}$ presents no evidence of a significant influence of the peripheral groups in the electronic transitions. The Soret band arise at 424 nm ($\varepsilon = 3.4 \times 10^5$ L cm^{-1} mol^{-1}) and the Q bands at 518 ($\varepsilon = 2.8 \times 10^4$ L cm^{-1} mol^{-1}), 554 ($\varepsilon = 1.2 \times 10^4$ L cm^{-1} mol^{-1}), 593 ($\varepsilon = 1.2 \times 10^4$ L cm^{-1} mol^{-1}) and 649 nm ($\varepsilon = 3.4 \times 10^5$ L cm^{-1} mol^{-1}). A band at 315 nm ($\varepsilon = 1.2 \times 10^4$ L cm^{-1} mol^{-1}) was attributed to a $\pi \rightarrow \pi^*$ transition of the ruthenium complex ligands. The spectra of the supramolecular species based on TThP and TMeThP show a 4 and 10 nm red-shift of the Soret band, respectively, but the molar absorptivities were more significantly affected (TThP derivative 428 nm ($\varepsilon = 2.2 \times 10^5$ L cm^{-1} mol^{-1}) and TMeThP derivative 434 nm ($\varepsilon = 4.8 \times 10^4$ L cm^{-1} mol^{-1})). Significant changes were also observed in the Q bands where the TThP derivative showed a small displacement concomitantly with a decrease in the molar absorptivity of these bands. In addition, three news bands were observed: a sharp and well-defined band appeared at 465 nm ($\varepsilon = 2.7 \times 10^4$ L cm^{-1} mol^{-1}), and at 660 and 718 nm, both with molar absorptivity around 7.0×10^3 L cm^{-1} mol^{-1}. In contrast, the Q bands of the TMeThP derivative were completely substituted by a broad and bathochromically shifted band centered at 747 nm ($\varepsilon \approx 9.0 \times 10^3$ L cm^{-1} mol^{-1}) and at 471 nm ($\varepsilon = 4.3 \times 10^4$ L cm^{-1} mol^{-1}). Interestingly, this new band is more intense than the Soret band. These bands were assigned supported by spectroelectrochemical analysis respectively to a $Ru^{II}(d\pi) \rightarrow p\pi^*$ of thienyl and 5,5′-Mebpy MLCT transitions, indicating a strong interaction between the porphyrin ring and the ruthenium complexes. Surprisingly, the cyclic voltammograms of these supermolecules presented two reversible monoelectronic processes at around −0.03 V, and a second one around 0.47 V (three electrons) suggesting a strong enough electronic coupling to separate the redox potentials of the peripheral ruthenium complexes in those two different values. This finding was studied using the electron paramagnetic resonance spectroscopy and coulometry techniques confirming that the first process refers to the oxidation of only one of the peripheral ruthenium complexes, while the more positive potential is related to the oxidation of the three other peripheral ruthenium complexes. In other words, in this system there is quite strong electronic communication between the ruthenium complexes through the porphyrin ring, made possible by the reduced steric hindrance of the five membered *meso*-thienyl rings of TThP, as compared to the larger six membered pyridyl ring of TPyP, allowing a more coplanar conformation.

Table II. Redox potentials (vs NHE) of tetraruthenated porphyrins.

Compounds	$P^{-/2-}$	$P^{0/-}$	$P^{0/+}$	$L^{-/2-}$	$L^{0/-}$	$Ru^{II/III}$	$M^{II/III}$	References
H_2(3-TRuP)	−1.06	−0.67	+1.57	−1.63[a)]	−1.39[a)]	+0.88	—	21
H_2(4-TRuP)	−0.93	−0.68	+1.65	−1.52[a)]	−1.38[a)]	+0.92	—	16
H_2(4-RuClphenP)	−1.04	−0.65	—	—	−1.11[b)]	+1.00	—	18
H_2(4-TRuoxP)	−1.04	−0.81	—	—	−1.34[c)]	+0.72	—	23
[Zn(3-TRuP)]	−1.17	−0.97	+1.31	−1.62[a)]	−1.38[a)]	+0.92	—	24
[Zn(4-TRuP)]	−1.18	−0.97	+1.31	−1.67 [a)]	−1.39 [a)]	+0.92	—	17
[Ni(4-TRuP)]	−0.97	−0.80	+1.57	−1.67[a)]	−1.37[a)]	+0.92	—	25
[Co(4-TRuP)]	—	—	—	−1.63[a)]	−1.39[a)]	+0.94	+0.1	26
[Fe(4-TRuP)]	—	−1.15	—	−1.63[a)]	−1.63[a)]	+0.94	+0.16	27
H_2(TRuPyViP)	−1.05	−0.70	—	—	—	+0.90	—	28
[Zn(TRuPyViP)	−1.21	−0.99	+1,43	—	—	+0.89	—	28

ligands: a) bpy. b) Clphen. c) Cl-tpy.

Table III. Redox potentials (vs NHE) of tetracluster porphyrins.

Compounds	$P^{-/2-}$	$P^{0/-}$	$P^{0/+}$	$M^{II/III}$	$Ru_3O^{2-/-}$	$Ru_3O^{0/-}$	$Ru_3O^{0/+}$	$Ru_3O^{0/2+}$	References
H_2(4-TCP)	−1.05	0.72	—	—	−1.14	+0.16	+1.23	+2.30	22
H_2(3-TCP)	−1.03	0.73	+1.55	—	−1.15	+0.17	+1.19	+2.21	22
Zn(4-TCP)	−1.27	−1.10	+1.35	—	−1.13	+0.15	+1.19	+2.18	19
Mn(4-TCP)	—	−0.94	—	+0.05	−1.17	+0.16	+1.17	≈+2.00	30
Co(4-TCP)	—	—	> +2.0	+0.31	−1.05	+0.16	+1.25	+2.33	29

$Ru_3O^{2-} = Ru^{III,II,II}$; $Ru_3O^{-} = Ru^{III,III,II}$; $Ru_3O^{0} = Ru^{III,III,III}$; $Ru_3O^{+} = Ru^{IV,III,III}$; $Ru_3O^{2+} = Ru^{IV,IV,III}$

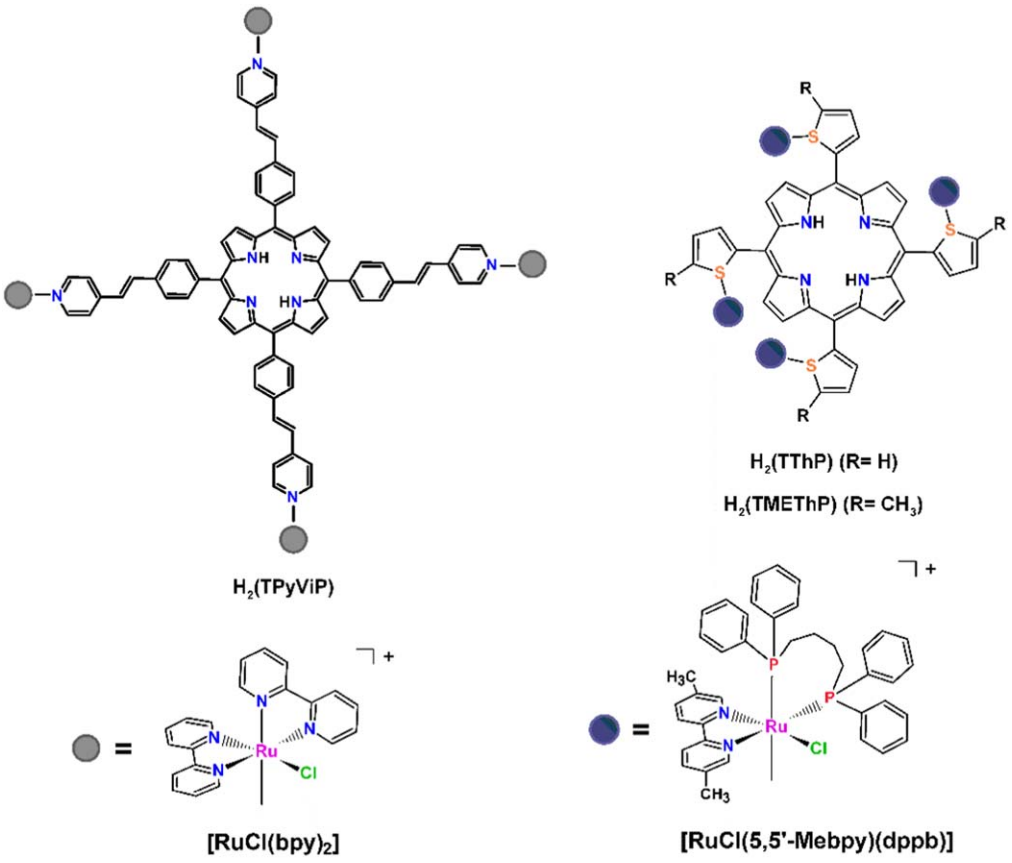

Figure 2. Structure of H_2(TPyViP), H_2(TThP) and H_2(TMeThP) porphyrins and it's tetraruthenated porphyrin species. The gray and violet spheres represent the peripheral coordination compounds.

Chemically modified electrodes as catalysts and electrochemical sensors

Conventional electrodes are transducers with characteristics limited by the intrinsic properties of the bulky material that are made of. However, new properties can be imparted to them by depositing different materials on the surface. In such modified electrodes the "conventional electrode" act as support and conducting material but the specific electrocatalytic properties are defined by the material deposited on the surface, making possible the creation of practically an infinite arsenal of new sensors. There are many procedures to modify electrodes, but probably electrodeposition, adsorption processes, covalent bonding and use of polymeric materials to entrap (or bond) the modifier to the electrode surface are the most relevant ones. The modifier materials can also be incorporated to the electrode as composites. Tetraruthenated porphyrins have low solubility in aqueous solution making the preparation of modified electrodes very easy, for example by drop casting.

As is well known, the application of molecular catalysts in homogeneous phase can be impaired by their low solubility in some common solvents. However, highly soluble molecular catalysts make their recycling difficult thus increasing the costs. In this sense, the heterogenization by immobilization of molecular catalysts on a solid substrate can potentially solve those problems since the obtained modified electrodes combine the high activity of molecular catalysts with the easy of recovery of heterogeneous materials. When catalysts are immobilized on electrodes surface for electrochemical and electroanalytical purposes, they are called chemically modified electrodes (CMEs).

CMEs have been the subject of considerable attention for more than four decades, when new materials and immobilization techniques were developed as the area greatly evolved. In fact, more robust and reproducible CMEs based on molecular catalysts can be achieved by **covalent** (anchoring by coordination and formation of covalent bonds with the substrate, and by electropolymerization) and **non-covalent immobilization** (insolubility immobilization, π-π interactions, electrostatic interactions) and by **periodic assembly method** (metal organic frameworks, porous organic polymers and

other similar hybrid materials).[37] The immobilization process should be carried out in such a way to transfer the physicochemical properties of the modifier to the electrode surface thus controlling the electrochemical behavior of the electrode/solution interface.[38] Generally, the non-covalent immobilization strategy relies on weaker van der Waals and π-π interactions of a molecular catalyst with the substrate, while the covalent strategy implies surface grafting or polymerization by chemical or electrochemical methods.[37] The periodic assembly method has been developed in recent years. The assembly of molecules into periodic porous skeletons deposited on the electrode surface can take place by space confinement in metal-organic frameworks and porous organic frameworks generating good heterogeneous catalysts and CMEs.

Nowadays the interest in CMEs has increased particularly to enhance the sensitivity and/or the selectivity of electroanalytical techniques. For example, Attatsi et al.[39] prepared CMEs by a **non-covalent immobilization** process transferring catalysts for fuel-producing reactions to the electrode surface. More specifically, a pyrene–pyridine hybrid (**Py–Py**) was used as axial ligand to bridge Co(II) *meso*-tetraphenylporphyrin (Fig. 3) which was adsorbed on carbon nanotubes via π-π interactions, generating a composite material that was finally used to modify glassy carbon electrodes. This axially coordinated Co(II)porphyrin significantly enhanced the rate of the oxygen reduction and oxygen evolution reactions, providing new insights to the understanding of catalysis by surface immobilized species.

On the other hand, Hu and co-workers[40] used the **covalent** strategy by electropolymerization for preparation of CMEs in a straightforward way, leading to the entrapment of an iron-porphyrin inside a microporous CO_2 absorbing material realizing a good electrocatalyst for CO_2 reduction. This was accomplished by oxidative electropolymerization on GC or ITO electrodes of a catalyst grafted with pendant carbazole substituents (Fig. 4). The film thickness and the surface coverage were precisely controlled by the number of voltammetric cycles. The iron-porphyrins served both as electrocatalyst and charge-transfer mediators by electron-hopping mechanism improving the conductivity of the polymeric film.

Another important way to prepare CMEs is by incorporation of the molecular catalysts into 2D metal organic frameworks[41] or 3D structured frameworks, such as covalent organic frameworks (COFs), or metal organic frameworks (MOFs), and other porous polymeric structures.[42,43] For instance, Zhang et al.[44] recently reported a material based on cobalt porphyrin ([Co(TCPP)] = (5,10,15,20)-tetrakis(4-carboxyphenyl)porphyrin-Co^{II}), that was prepared by precisely anchoring that molecule onto water-stable 2D metal–organic framework (MOF) nanosheets (Zr-BTB). The material is constituted by ultrathin 2D MOF nanosheets ([Co(TCPP)]/Zr-BTB) with accessible catalytic active sites for CO_2 reduction reaction (Fig. 5). The [Co(TCPP)]/Zr-BTB exhibited ultrahigh turnover frequency (TOF = 4768 h^{-1}) at −0.919 V *vs* reversible hydrogen electrode (RHE) owing to the high active-site utilization as compared with the cobalt porphyrin precursor. In addition, three 2D MOF nanosheets ([Co(TCPP)]/Zr-BTB-PABA, [Co(TCPP)]/Zr-BTB-PSBA, [Co(TCPP)]/Zr-BTB-PSABA) were post-modified with *p*-(aminomethyl)benzoic acid (PABA), *p*-sulfobenzoic acid (PSBA), and *p*-sulfamidobenzoic acid (PSABA) by coordination and hydrogen bonding interactions, to control the steric properties around the [Co(TCPP)]. Among them, the [Co(TCPP)]/Zr-BTB-PSABA conjugate exhibited the best electrocatalytic performance presenting a faradaic efficiency of 85.1%, TOF of 5315 h^{-1}, and j_{total} of 6 mA cm^{-2} at −0.769 V (*vs* RHE), for reduction of CO_2 to CO.

Electrocatalysts Based on Tetraruthenated Porphyrins

Molecular catalysts based on macrocycles have been intensively studied in the last two decades, mainly heterogeneous molecular catalysts based on metalloporphyrins macrocycles. In fact, these molecular catalysts often deliver higher performance and selectivity than classical metallic solid-state catalysts, even in unfavorable

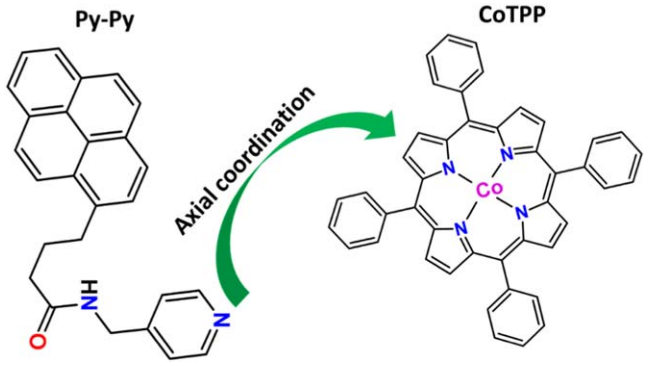

Figure 3. Scheme showing the structures of the pyrene—pyridine hybrid (Py–Py) used as axial ligand to bridge Co(II) meso-tetraphenylporphyrin.

aqueous environments.[45] In addition, molecular catalysts can present poor solubility in some common solvents, responsible for low percentage of utilization of the active sites and difficulty in recycling when used in homogeneous catalytic systems, problems that can be solved by immobilization.[37] In this context, Sun et al.[37] recently summarized the methods that have been developed so far for anchoring of homogeneous molecular catalysts on an electrode surface, and reported the challenges and factors affecting the electrocatalytic activity for CO_2 reduction.

Gotico and collaborators[46] reviewed the recent advances in the design of metalloporphyrin-based heterogenized catalysts for CO_2 reduction. In addition, Elouarzaki et al.[45] considered the recent state-of-the-art molecular catalysts for CO_2 electroreduction and explained their performances, therefore providing the design principles for the next generation of hybrid molecular material. However, despite the recently published review works,[47–49] no one mentioned the recent advances based on **tetraruthenated porphyrins (TRuPs)** as electrocatalysts or photoelectrocatalysts for reduction of CO_2 or other molecules of environmental interest. In fact, TRuPs have been applied as catalysts for various reactions, for example, hydroxylation of cyclohexane,[50] epoxidation[50] and oxidation of cyclohexene[51] and reduction of O_2.[34,52–56] However, as will be shown below, a growing interest in the development of CMEs for reduction of CO_2 and NO_2^- has been observed, the focus of the next topics.

TRuP-based electro and photoelectrocatalysts for CO_2 reduction.—The development of molecular catalysts for the selective transformation of CO_2 to reduced carbon species is gathering an enormous interest[46] and is one of the key areas of research for achieving electrical-to-chemical energy storage and feedstock chemical synthesis.[45] In this sense, some **TRuPs-**based electrocatalysts have been reported as being efficient in converting CO_2 into several products. For example, García et al.[57] studied electrochemical and photoelectrochemical reduction of CO_2 in aqueous solution, using an multilayer modified ITO electrode. Multiple layers of molecular catalysts were deposited by a non-covalent Layer-by-Layer method (LBL), using a TRuP coordinated to Mn(III), Zn(II) and Ni(II) in the macrocyclic cavity ($[Mn^{III}(TRuP)]^{5+}$, $[Zn^{II}(TRuP)]^{4+}$ and $[Ni^{II}(TRuP)]^{4+}$, respectively) and an anionic polyoxotungstate $[SiW_{12}O_{40}]^{4-}$, as confirmed by electrochemical methods and UV–visible spectroscopy[58] CO_2 reduction was investigated by linear sweep voltammetry at pseudo stationary state (5 mV s^{-1}) in a CO_2 saturated 0.1 M $NaClO_4$ solution. Carbon dioxide reduction by $[Mn^{III}(TRuP)]^{5+}/[SiW_{12}O_{40}]^{4-}$, $[Zn^{II}(TRuP)]^{4+}/[SiW_{12}O_{40}]^{4-}$ and $[Ni^{II}TRuP]^{5+}/[SiW_{12}O_{40}]^{4-}$ modified electrodes exhibited an onset potential of −0.6 V, −0.65 V and −0.6 V vs Ag/AgCl, respectively, and the peak current intensities decreased in the order $[Mn^{III}(TRuP)]^{5+}/[SiW_{12}O_{40}]^{4-} > [Ni^{II}(TRuP)]^{4+}/[SiW_{12}O_{40}]^{4-} > [Zn^{II}TRuP]^{4+}/[SiW_{12}O_{40}]^{4-}$. As it can be seen in Table IV, the $[Mn^{III}(TRuP)]^{5+}/[SiW_{12}O_{40}]^{4-}$ multilayer modified electrode showed the largest TOF and TON values for formic acid production,

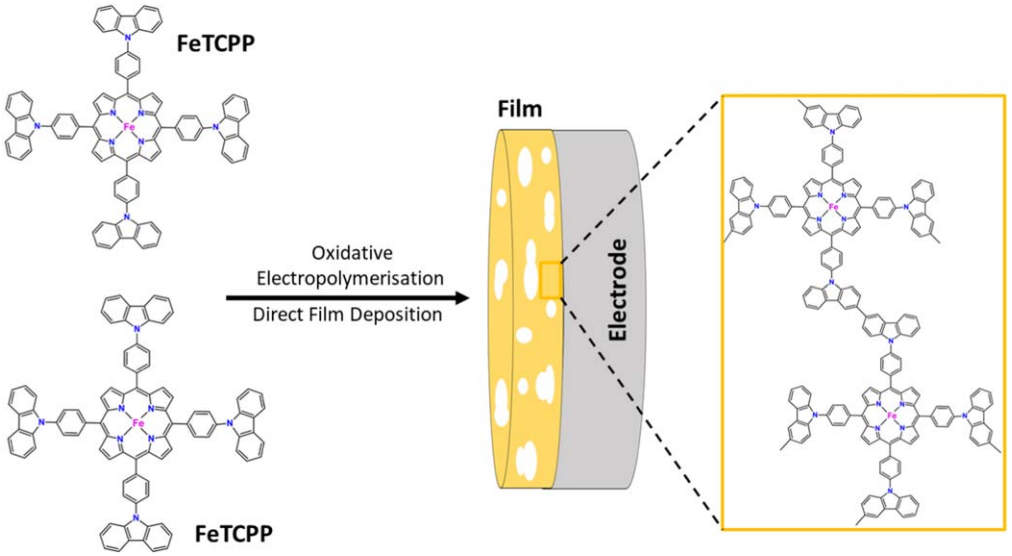

Figure 4. Scheme showing the covalent strategy by film formation via oxidation electropolymerization of FeTCPP.[37,40]

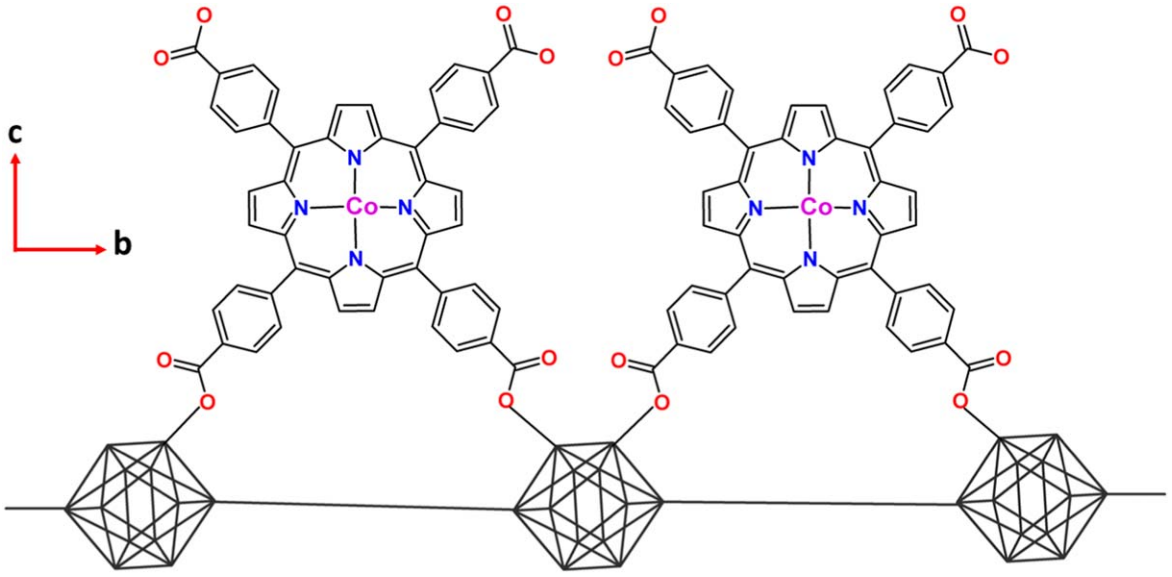

Figure 5. Simplified scheme showing the structure of the crystal structure of TCPP(Co)/Zr-BTB nanosheets along the a axis obtained by incorporation of the molecular catalysts into 2D metal organic frameworks.[44]

while $[Zn^{II}(TRuP)]^{4+}/[SiW_{12}O_{40}]^{4-}$ multilayer modified electrodes exhibit the best TOF and TON values for methanol production.

The possibility of photoelectrochemical CO_2 reduction was evaluated in the same experimental conditions described above under irradiation with 440 nm light with minimal shift to −0.60 V. Nevertheless, there was a change in the product distribution, and formaldehyde was detected for the manganese and zinc derivatives, evidencing a change in the reduction mechanism. For example, formaldehyde was the only product using $[Mn^{III}(TRuP)]^{5+}/[SiW_{12}O_{40}]^{4-}$ modified electrodes under irradiation, in contrast with formic acid and methanol generated in dark conditions. $[Ni^{II}(TRuP)]^{4+}/[SiW_{12}O_{40}]^{4-}$ modified electrodes exhibited a similar behavior. On the other hand, the amount of formic acid produced with $[Zn^{II}(TRuP)]^{4+}/[SiW_{12}O_{40}]^{4-}$ multilayer modified electrodes under photoelectrochemical conditions was 12 fold larger than in dark conditions. Accordingly, formic acid production is favored under irradiation but the methanol production depends solely on the applied potential.

Calfumán and collaborators[59] studied the electrochemical reduction of CO_2 in aqueous solution mediated by Co^{2+} and Zn^{2+} TRuP in Nafion (Nf) and polyvinyl chloride (PVC) as support to immobilize and improve the properties of those molecular electrocatalysts. The influence of the two polymeric matrices were evaluated comparing the electrocatalytic performance of GC/PVC/[M(TRuP)] and GC/Nf/[M(TRuP)] for CO_2 reduction, at −600 mV *vs* Ag/AgCl. Interestingly, the TOF value for GC/PVC/[Co(TRuP)] was 44 times larger than for the zinc analogue with Nf considering the production of formaldehyde (formic acid was also produced using both matrices) but [Zn(TRuP)] modified electrodes produced more CH_3OH overall. As shown in Table IV, TOF values obtained for GC/Nf/[Zn(TRuP)] were about 0.03 s^{-1}, while GC/PVC/[Zn(TRuP)] was more efficient reaching 1.63 s^{-1} largely due to H_2CO production. In general, the best results were obtained with PVC/M(TRuP), while electrodes modified with Nafion/[M(TRuP)] were less specific but produced larger amounts of product. One possible reason was the agglomeration of [M(TRuP)] in PVC generating regular knots (entangled polymer chains) on the electrode surface.[60] Thus, agglomerated [M(TRuP)] seems to increase the selectivity of the electrocatalysts while increasing the rugosity of the film, speeding up the electron transfer processes in the PVC system.[60]

Table IV. Activity parameters of recently reported TRuP based electrocatalysts: electrolysis conditions, faradaic efficiencies, TOF, TON and pH conditions.

Electrocatalysts	Substrate	Reaction products	Conditions electrolysis (V)	Faradaic efficience (%)	TOF (s^{-1})	TON	pH condition	References
GC/Nf/[Co(TRuP)]	CO_2	HCOH		64.1	0.23			
		HCOOH	−1.0	5.6	0.03	—	4.2	59
		CH_3OH		8.4	0.09			
GC/Nf/[Zn(TRuP)]	CO_2	HCOH		57.2	0.37			
		HCOOH	−1.0	4.4	0.09	—	4.2	59
		CH_3OH		—	0			
GC/PVC/[Co(TRuP)]	CO_2	HCOH		21.2	1.31			
		HCOOH	−1.0	0.04	0.04	—	4.2	59
		CH_3OH		—	0			
GC/PVC/[Zn(TRuP)]	CO_2	HCOH		—	—			
		HCOOH	−1.0	—	0	—	4.2	59
		CH_3OH		25.7	0.88			
$[Mn^{III}(TRuP)]^{5+}/[SiW_{12}O_{40}]^{4-}$	CO_2	HCOOH		—	4.8×10^{-1}	1.06×10^4	0.1 M	57
		CH_3OH	−0.75	—	2.3×10^{-2}	5.0×10^2	$NaClO_4$	
		CO		—	—	—		
$[Zn^{II}(TRuP)]^{4+}/[SiW_{12}O_{40}]^{4-}$	CO_2	HCOOH		—	3.7×10^{-3}	8.3	0.1 M	
		CH_3OH	−0.75	—	8.2	1.76×10^5	$NaClO_4$	57
		CO		—	—	—		
$[Ni^{II}(TRuP)]^{4+}/[SiW_{12}O_{40}]^{4-}$	CO_2	HCOOH		—	8.3×10^{-2}	1.8×10^3	0.1 M	
		CH_3OH	−0.75	—	—	—	$NaClO_4$	57
		CO		—	2.4×10^{-1}	3.85×10^3		
$[Mn^{III}(TRuP)]^{5+}/[SiW_{12}O_{40}]^{4-}$	NO_2^-	NH_2OH		24.98	4.7	148.8	0.1 M	
		N_2H_2	−0.8 V	48.84	11.5	363.9	$NaClO_4$	67
		NH_3	(*vs* Ag/AgCl)	21.95	3.4	109.2	pH = 5.7	
$[Zn^{II}(TRuP)]^{4+}/[SiW_{12}O_{40}]^{4-}$	NO_2^-	NH_2OH		28.06	3.8	122.6	0.1 M	
		N_2H_2	−0.8 V	53.03	9.0	288.5	$NaClO_4$	67
		NH_3	(*vs* Ag/AgCl)	35.26	4.0	128.0	pH = 5.7	
$[Ni^{II}(TRuP)]^{4+}/[SiW_{12}O_{40}]^{4-}$	NO_2^-	NH_2OH		21.01	3.2	100.6	0.1 M	
		N_2H_2	−0.8 V	34.40	6.5	288.5	$NaClO_4$	67
		NH_3	(*vs* Ag/AgCl)	35.97	4.5	143.0	pH = 5.7	
$[SiW_{12}O_{40}]^{4-}/[Zn^{II}(TRuP)]^{4+}$	NO_2^-	NH_2OH		—	—	—	0.1 M	67
		N_2H_2	−0.8 V	38.88	2.4	129.3	$NaClO_4$	
		NH_3	(*vs* Ag/AgCl)	24.56	1.9	2.51×10^5	pH = 5.7	
GC/PVC/[Co(TRuP)]	NO_2^-	NH_2OH		—	12230	—		
		N_2H_2	−1.0	—	6934	—	0.1 M $NaClO_4$	60
		NH_3		—	12434	—	pH = 6	
GC/PVC/[Ni(TRuP)]	NO_2^-	NH_2OH		—	6005	—	0.1 M	
		N_2H_2	−1.0	—	3561	—	$NaClO_4$	60

Table IV. (Continued).

Electrocatalysts	Substrate	Reaction products	Conditions electrolysis (V)	Faradaic efficience (%)	TOF (s^{-1})	TON	pH condition	References
		NH_3		—	6673	—	pH = 6	
GC/PVC/[Zn(TRuP)]	NO_2^-	NH_2OH		—	7168	—	0.1 M	
		N_2H_2	−1.0	—	5128	—	$NaClO_4$	60
		NH_3		—	8867	—	pH = 6	
GC/Nf/[Co(TRuP)]	NO_2^-	NH_2OH		—	9388	—	0.1 M	
		N_2H_2	−1.0	—	1717	—	$NaClO_4$	65
		NH_3		—	3171	—	pH = 6	
GC/Nf/[Ni(TRuP)]	NO_2^-	NH_2OH		—	3921	—	0.1 M	
		N_2H_2	−1.0	—	809	—	$NaClO_4$	65
		NH_3		—	1110	—	pH = 6	
GC/Nf/[Zn(TRuP)]	NO_2^-	NH_2OH		—	2994	—	0.1 M	
		N_2H_2	−1.0	—	709	—	$NaClO_4$	65
		NH_3		—	853	—	pH = 6	
H_2(TRuP)	NO_2^-	NH_2OH		—	~260	—	0.1 M	
		N_2H_2	$-1.2^{\#}$	—	~35	—	$NaClO_4$	69
		NH_3		—	~20	—	pH = 5.9	
[Ni(TRuP)]	NO_2^-	NH_2OH		—	~30	—	0.1 M	
		N_2H_2	$-1.2^{\#}$	—	~5	—	$NaClO_4$	69
		NH_3		—	~2.5	—	pH = 5.9	
[Zn(TRuP)]	NO_2^-	NH_2OH		—	~120	—	0.1 M	
		N_2H_2	$-1.2^{\#}$	—	~14	—	$NaClO_4$	69
		NH_3		—	~15	—	pH = 5.9	
$\{[Ni(TPyP)[Ru(NO_2—phen)_2Cl_4]^{4+}\}$	NO_2^-	NH_2OH		—	30.2	—	0.1 M	
		N_2H_2	−0.4	—	4.2	—	$NaClO_4$	68
		NH_3		—	7.1	—	pH = 6	

= Other potential values for electrocatalytic activities have been reposted, PVC = polyvinyl chloride, Nf = Nafion, GC = Glassy Carbon.

Electrochemical impedance measurements corroborate and explain the higher TOF of GC/PVC/[M(TRuP)] as compared to GC/Nf/[M(TRuP)] (where M = Zn^{2+} and Co^{2+}) modified electrodes. Electrochemical impedance spectroscopy showed that PVC electrodes present a non-uniform surface with variable impedance zones resulting in high capacitances that compensate the slow electrochemical reactions. Those capacitances are associated with three relaxation times, consistent with three different charge storage sites or, in other words, three active sites for reaction. This results are consistent with the high TOF measured for GC/PVC/[Zn(TRuP)], suggesting that PVC/[Zn(TRuP)] are good candidates as components of Membrane Assembled Electrodes, and a system for continuous reduction of carbon dioxide.

TRuP-based electro and photoelectrocatalysts for nitrite reduction.—In addition to excellent catalysts for CO_2 reduction, the previously reported modified electrodes were also used as electro and photoelectrocatalysts for nitrite reduction (NO_2^-). Nitrite is an ubiquitous pollutant in modern society because of its excessive use as preservative in meat, processed foods and beverages, since cause eutrophication when reach water bodies and can pose a serious health risk[61] such as methaemoglobinemia. In this case, nitrite oxidize Fe^{2+} present in hemoglobin (Hb) to Fe^{3+} generating methaemoglobin (metHb) which is incapable of performing its physiologic function.[62] Besides, nitrite can generate carcinogenic agents denominated N-nitrosamines by combination with amines, as mentioned by the International Association for Research on Cancer (IARC).[63] In this sense, the removal or conversion of nitrite and nitrate in water to harmless compounds, is one of the current goals in environmental remediation.

Aiming at this application, García et al.[60] also performed the electro and photoelectrochemical reduction of nitrite in aqueous solution, using ITO electrodes modified with $[M(TRuP)]^{n+}/[SiW_{12}O_{40}]^{4-}$ by LBL method (M = Mn^{3+}, Zn^{2+} and Ni^{2+}) as multielectrocatalysts. Analogously to the work cited above, NO_2^- reduction on these electrode surface was investigated in dark conditions and under light irradiation, where the onset potentials for NO_2^- reduction at $[Mn^{III}(TRuP)]^{5+}/[SiW_{12}O_{40}]^{4-}$, $[Zn^{II}(TRuP)]^{4+}/[SiW_{12}O_{40}]^{4-}$ and $[Ni^{II}(TRuP)]^{4+}/[SiW_{12}O_{40}]^{4-}$ modified electrodes were respectively −0.35, −0.4 and −0.65 V. The current value for nitrite reduction, at −0.8 V *vs* Ag/AgCl, followed the trend $[Ni^{II}(TRuP)]^{4+}/[SiW_{12}O_{40}]^{4-}$ > $[Zn^{II}(TRuP)]^{4+}/[SiW_{12}O_{40}]^{4-}$ > $[Mn^{III}(TRuP)]^{5+}/[SiW_{12}O_{40}]^{4-}$. In addition, hydroxylamine, hydrazine and ammonia were the reduction products in the dark, under controlled potential electrolysis conditions. At constant potential, the molar concentration of hydroxylamine and hydrazine decreased in the order $[Mn^{III}(TRuP)]^{5+}/[SiW_{12}O_{40}]^{4-}$ > $[Zn^{II}(TRuP)]^{4+}/[SiW_{12}O_{40}]^{4-}$ > $[Ni^{II}(TRuP)]^{4+}/[SiW_{12}O_{40}]^{4-}$ (in the case of ammonia, the order was reversed). The relevant parameters TOF, TON and faradaic efficiency for nitrite reduction were summarized in Table IV. Note that in all cases, the trend is the same as that observed for the total amount of reaction products obtained in the potentiostatic electrolysis. Finally, it is important to mention that only hydrazine and ammonia could be detected as reduction products using the $[SiW_{12}O_{40}]^{4-}/[Zn^{II}(TRuP)]^{4+}$ CME.

Under light irradiation, only hydrazine and ammonia were found and, the authors observed an increase in the total amount of products (Table V). In this case, the electrolysis was carried out at −0.65 V *vs* Ag/AgCl, and required half of the time than in dark conditions. These results showed that the combination of light and electrical potential can improve the electrocatalytic properties of the modified electrodes. In fact, the largest amount of hydrazine was produced using the $[Zn^{II}(TRuP)]^{4+}/[SiW_{12}O_{40}]^{4-}$ modified electrode under light irradiation, followed by $[Mn^{III}(TRuP)]^{5+}/[SiW_{12}O_{40}]^{4-}$, $[Ni^{II}(TRuP)]^{4+}/[SiW_{12}O_{40}]^{4-}$ and the bare ITO electrode. $[Mn^{III}(TRuP)]^{5+}/[SiW_{12}O_{40}]^{4-}$ CME produced three times more hydrazine under photoelectrochemical than in dark conditions, whereas $[Zn^{II}(TRuP)]^{4+}/[SiW_{12}O_{40}]^{4-}$ and $[Ni^{II}(TRuP)]^{4+}/[SiW_{12}O_{40}]^{4-}$ modified electrodes showed an enhancement of 6 and 5 times respectively. These results are consistent with the increase of 1–2 order of magnitude of TOF values and 4 orders of magnitude of TON values, demonstrating the very positive effect induced by light (see Table V).

Interestingly, $[Mn^{III}(TRuP)]^{5+}/[SiW_{12}O_{40}]^{4-}$ modified electrodes were more efficient in producing ammonia than $[Zn^{II}(TRuP)]^{4+}/[SiW_{12}O_{40}]^{4-}$ > $[Ni^{II}(TRuP)]^{4+}/[SiW_{12}O_{40}]^{4-}$ > bare ITO electrode. Compared to dark conditions, ammonia production doubled with the $[Mn^{III}(TRuP)]^{5+}/[SiW_{12}O_{40}]^{4-}$ modified electrodes, increased 1.4 times with the $[Zn^{II}(TRuP)]^{4+}/[SiW_{12}O_{40}]^{4-}$ and no significant effect was observed for $[Ni^{II}(TRuP)]^{4+}/[SiW_{12}O_{40}]^{4-}$ modified electrodes. TOF values also increased one order of magnitude and TON increased 3 orders of magnitude, following the same trend. Nearly 90% overall faradaic efficiency was achieved showing that the combination of light and electrochemical potential generates highly protonated products in detriment of gaseous products. These results are consistent with the hypothesis of a synergic effect of photocatalysis and electrocatalysis, leading to improved photoelectrocatalytic behavior. The applied potential facilitates the separation of photo-induced carriers while light absorption lowers the energetic barrier for electron transfer.[64]

Much more promising results were reported by Calfumán et al.[65] for the electrochemical reduction of nitrite in neutral aqueous solution mediated by [M(TRuP) (M = Co^{2+}, Ni^{2+} and Zn^{2+}) electrostatically assembled onto a Nafion film, previously adsorbed on ITO or glassy carbon electrodes. The macrocyclic complexes form multiple layers with disordered stacking orientation on the Nafion occupying hydrophobic and hydrophilic sites in the polyelectrolyte film, as confirmed by scanning electron microscopy (SEM-EDX) and transmission electron microscopy (TEM).[65]

These CMEs were able to reduce nitrite at −660 mV showing enhanced currents and a significantly lower overpotential as compared to bare GCE. Among the metallated derivatives, the [Co(TRuP)] modified electrode was the most efficient one, as demonstrated by scanning electrochemical microscopy (SECM) images. Controlled potential electrolysis experiments at −1 V confirmed the production of ammonia, hydrazine and hydroxylamine demonstrating some selectivity and stability for reduction of the nitrite ion. In fact, the TOF for ammonia production is almost a third of hydroxylamine while the TOF for hydrazine is less important. Also, the TOF of the modified electrodes (Table IV) presented the following order: GC/Nf/[Co(TRuP)] ⩾ GC/Nf/[Ni(TRuP)] > GC/Nf/[Zn(TRuP)]. As mentioned before, the GC/Nf/[Co(TRuP)] modified electrodes exhibited the highest catalytic activity shedding light on the nature of the active site of these electrocatalyst. It is possible that the reduction of NO_2^- on GC/Nf/ZnTRP and GC/Nf/NiTRP modified electrodes is activated by electron-transfer from a reduced porphyrin ring where the metallic center may play minor role.[18] In the case of [Co(TRuP)], it has been demonstrated that the analogous Co(III)-*meso*-tetra(4-methyl-pyridynium)porphyrin [Co(TMPyP)] (i.e. the macrocycle where the Ru(II) moieties are replaced by $-CH_3$ groups) can coordinate NO_2^- in aqueous solution at pH 4.7[66] presenting a rate constant of 8.4 ± 02 $M^{-1}\,s^{-1}$. Furthermore, the formation of reduced nitrite products catalyzed by that macrocycle was demonstrated upon addition of several reductants[65]

In addition to Nafion, Calfumán and collaborators[60] also employed GC electrodes modified with tetraruthenated metalloporphyrins immobilized on PVC for electrochemical reduction of nitrite (GC/PVC/[M(TRuP)). These modified electrodes exhibited good electrocatalytic activity in pH 6 aqueous media. The investigations using voltammetry showed an enhancement in the current values and lower overpotential as compared with the bare glassy carbon electrode, and electrodes modified with Nf/[Ni(TRuP)][65] and $[M(TRuP)]^{n+}/[SiW_{12}O_{40}]^{4-}$.[58,67] Controlled potential electrolysis experiments were carried out demonstrating the production of ammonia, hydrazine and hydroxylamine even at very negative potentials. The onset potential was −350 mV for [Co(TRuP)] and

Table V. Activity parameters of recently reported TRuP based photoelectrocatalysts: electrolysis conditions, faradaic efficiencies, TOF, TON and pH conditions.

Photoelectrocatalysts	Substrate	Reaction products	Onset potential (V *vs* RHE)	Faradaic efficience(%)	TOF (s^{-1})	TOM	$[Conc.]_{50\%}$ (h)	pH condition	References
H_2(TRuP)/PMA	Methyl Orange @	—	—	—	—	—	50.5	—	73
$[Mn^{III}(TRuP)]^{5+}/[SiW_{12}O_{40}]^{4-}$	NO_2^-	N_2H_2	−0.65 V	71.49	100.8	1.6×10^6	—		67
		NH_3	(*vs* Ag/AgCl)	21.15	19.9	3.15×10^5			
$[Zn^{II}(TRuP)]^{4+}/[SiW_{12}O_{40}]^{4-}$	NO_2^-	N_2H_2	−0.65 V	55.72	155.4	2.4×10^6	—		67
		NH_3	(*vs* Ag/AgCl)	52.23	15.5	2.4×10^5			
$[Ni^{II}(TRuP)]^{4+}/[SiW_{12}O_{40}]^{4-}$	NO_2^-	N_2H_2	−0.65 V	19.44	83.8	1.3×10^6	—		67
		NH_3	(*vs* Ag/AgCl)	22.60	13.6	2.1×10^5			
$[Mn^{III}(TRuP)]^{5+}/[SiW_{12}O_{40}]^{4-}$	CO_2	HCOOH	−0.65 V	—	—	—	—	0.1 M $NaClO_4$	57
		CH_3OH	(*vs* Ag/AgCl)	—	—	—			
		HCOH		—	16.7	1.8×10^5			
$[Zn^{II}(TRuP)]^{4+}/[SiW_{12}O_{40}]^{4-}$	CO_2	HCOOH	−0.65 V	—	1.3×10^{-1}	1.4×10^3	—	0.1 M $NaClO_4$	57
		CH_3OH	(*vs* Ag/AgCl)	—	7.3×10^{-1}	7.9×10^3			
		HCOH		—	—	—			
$[Ni^{II}(TRuP)]^{4+}/[SiW_{12}O_{40}]^{4-}$	CO_2	HCOOH	−0.65 V	—	—	—	—	0.1 M $NaClO_4$	57
		CH_3OH		—	—	—			
		HCOH	(*vs* Ag/AgCl)	—	1.78	3.85×10^4			

@ = photo-oxidation, # = Other potential values for electrocatalytic activities have been reposted, PVC = polyvinyl chloride, Nf = Nafion, GC = Glassy Carbon.

−530 mV for [Ni(TRuP)] and [Zn(TRuP)], demonstrating the higher electrocatalytic activity of the cobalt derivative and the stability of this modified electrode, that decreased in the order GC/PVC/[Co (TRuP)] > GC/PVC/[Zn(TRuP)] ⩾ GC/PVC/[Ni(TRuP)]. It is also important to note that the high TOF for production of NH_2OH, N_2H_2 and NH_3 outperformed the results obtained for $\{[Ni(TPyP)[Ru(NO_2\text{-phen})_2Cl_4]^{4+}\}$[68] ($NO_2$-phen = 5-Nitro-1,10-phenanthroline), H_2TRuP, NiTRuP and ZnTRuP[69] modified electrodes, as shown in Table IV.

Worth mentioning that the Zn^{2+} complex is more active than the Ni^{2+} complex. This fact can shed some light regarding the nature of the active site of the catalyst. It has been shown[70,71] that open shell transition metals are active toward the reduction, because they are able to form an intermediary complex before the electron transfer, or bind the analyte in a lower oxidation state. It is well known that Zn^{2+} does not present such a property, since it is a closed shell d^{10} transition metal ion. Thus, it is very possible that the reduction of nitrite would be activated for an electron transfer from a reduced macrocycle ring without the intervention of the metallic ion center.[18,72] Therefore Co^{2+} center can provide a more stable reduced catalytic active macrocycle species for nitrite reduction, following the same mechanism observed for Nf/[Co(TRuP)] modified electrodes.[65]

Chemical Sensor Based on Tetraruthenated Porphyrins

Among the molecular species used as electrode surface modifying agents, porphyrins have stood out due to their ease of immobilization on the electrode surface, as well as their electrocatalytic characteristics, as summarized in Table VI where some examples of electrochemical sensors are presented. Indeed, porphyrins have a very rich electrochemical behavior with many oxidation and reduction processes, associated with the porphyrin ring and different substituents that can be bound to the *meso* and/or pyrrolic beta-positions. Besides, the internal pyrrolic hydrogen atoms of porphyrins can be removed to form the porphyrinate ligand, and transition metal ions can be coordinated to the four nitrogen atoms in the cavity, thus providing another active electrocatalytic site.

In this context, Araki and collaborators have demonstrated over the years that metalloporphyrins based on *meso*-tetra(pyridyl)porphyrins, H_2TPyP, when coordinated with transition metal complexes such as $[Ru(bipy)_2Cl]^+$, $[Ru(NH_3)_5]^{2+}$ and $[Ru(edta)]^{-1}$, not only have their chemical properties changed but the solubility and molecular interactions were also modified, allowing the deposition of these materials as thin and compact films on the electrode surface.

The modified electrodes cited above have been used as amperometric or voltammetric sensors for many analytes with environmental and pharmaceutical interest.[26,74–76] But, although these electrodes do not show evidence of poisoning by the analytes, these films are relatively soluble in aqueous media, a characteristic which may lead to a decrease in the amperometric response. To eliminate this disadvantage, the subtopics below will show the main molecular immobilization strategies for the development of CMEs, mainly applying TRuPs and composites as electrochemical sensors.

TRuP-based CMEs prepared by noncovalent immobilization.— In order to circumvent the leaching/solubilization process, Araki and collaborators developed an interesting noncovalent immobilization strategy based on **layer-by-layer** formation of insoluble ion-paired porphyrin films,[77] by which homogeneous and compact thin films were prepared by transferring a cationic porphyrin solubilized in methanol, onto the electrode surface and dried at room temperature. Then, an amount of anionic porphyrin aqueous solution was deposited onto the modified electrode, and the excess removed with deionized water. This process can be repeated several times until obtaining a film with desired thickness. The cationic, anionic and ion-paired porphyrins structures are presented in Fig. 6. Even though these films present the same electrochemical behavior of electrodes modified only with [M(TRuP)], they have the advantage of being more reproducible and more stable in aqueous media.

In fact, da Rocha et al.[78] using a FIA/amperometric system and a CME with ion-paired CoTRuP/ZnTPPS, where CoTRuP is *meso*-tetra(4-pyridyl)porphyrinato cobalt(III) coordinated to four $[Ru(bipy)_2Cl]^+$ groups and ZnTPPS is *meso*-tetra (4-sulphonatephenyl) porphyrinato zinc(II), determined nitrite in saliva samples. The electrochemical behavior of that electrode was verified by cyclic voltammetry, in the 0.25–1.0 V *vs* Ag/AgCl range, in the absence and presence of increasing concentrations of nitrite ion. The CME presented an anodic (0.75 V) and cathodic wave (0.66 V) associated with the Ru^{II}/Ru^{III} redox process. In the presence of nitrite ion, an increase of anodic current was observed at the region of the Ru^{II}/Ru^{III} redox process. Accordingly, the working potential of 0.75 V was chosen to be applied at the modified electrode for determination of nitrite in saliva samples. It is worth noting that even after 25 days the CoTRuP/ZnTPPS electrode presented the same electrochemical behavior, demonstrating that the noncovalent immobilization strategy through formation of ion-paired porphyrins prevents the leaching/solubilization of the molecular material.

Similarly, Martins et al.[79] using a compact system encompassing a diffusion gas unit and an amperometric FIA detector based on a ion-paired porphyrin film (ZnTRuP/FeTPPS), determined sulfite ion in industrialized concentrated juices and coconut water, and this method was compared to the standard Monnier-Williams method. The electrochemical behavior of ZnTRuP/FeTPPS electrode in aqueous media was similar to of other tetraruthenated porphyrin CMEs; and the working potential for sulfite analysis was determined first by cyclic voltammetry and then by FIA/amperometric method, keeping the working potential constant at +0.9 V *vs* Ag/AgCl (potential is related to the $Ru^{II/III}$ process). The FIA/amperometric method showed a linear response between 0.64 and 6.4 ppm of sodium sulfite, limit of detection (LOD) 0.5 μM, relative standard deviation ±1.5% and analytical frequency 85 analyses h^{-1}. Thus, the FIA/amperometric method was shown to be an interesting alternative to time-consuming Monnier-Williams method since make possible faster, more reproducible and accurate analyses of sulfite in concentrated juices.

TRuP-based CMEs prepared by covalent immobilization.— Another interesting strategy to immobilize the porphyrin on electrode surface was developed by Winnishofer et al.[18] where a methanolic solution of a tetraruthenated porphyrin with four $[Ru(5\text{-ClPhen})_2Cl]^+$ groups attached to the pyridine N-atoms of H_2(4-TPyP) was transferred onto GCE surface and then electropolymerized (one of the covalent immobilization methods) by scanning the potentials in the 0.0 to −1.3 V vs SHE (Standard Hydrogen Electrode) range. Interestingly, the electropolymerized material exhibited a heterogeneous electron-transfer rate constant of $k_f = 6.2 \pm 0.1 \times 10^4\ M^{-1}\ s^{-1}$, 22 times higher than of similar ion-paired porphyrin ($k_f = 2.7 \times 10^3\ M^{-1}\ s^{-1}$), suggesting that the electropolymerized porphyrin is a much better electrocatalyst for nitrite oxidation to nitrate than the corresponding electrostatically ion-paired material. Another advantage is the easy control of film thickness, in which a surface concentration larger than 1.2×10^{-8} mol cm^{-2} was shown to increase the electrolyte diffusion impedance in the porphyrin film.

Using a similar strategy, Quintino et al.[80] electropolymerized a Ni(II) tetraruthenated porphyrin, named [NiTRuP], on GCE surface, and the modified electrodes were used as electrochemical sensors for glucose in alkaline medium. Poly[NiTRuP] was obtained by successive cyclic scans in [NiTRuP] in 0.1 M NaOH solution, in the 0.0 to 0.9 V *vs* Ag/AgCl range. The formation of poly[NiTRuP] was strongly influenced by the potential window. In fact, when the final potential was less than 0.9 V, the electropolymerized material was not formed. However, when the final potential was equal to or higher than 0.9 V, the growth of the electropolymerized film was easily observed in the successive cyclic voltammograms. It is worth mentioning that the electrocatalytic active site for glucose oxidation

Table VI. Electrochemical sensors based on porphyrins and some electroanalytical parameters.

Analyte	Sensor	Substrate	Method	Linear range	LOD	Sensitivity	References
Nitrite	CoTRuP/ZnTPPS	GCE	FIA/Amperometric	1–9 μM	0.1 μM	0.9 nA μM^{-1}	78
	$CoTMPyP/SrTa_2O_7$	GCE	DPV	0.29–3.31 mM	14 μM	—	95
	Co(II)MTpAP/cit-AuNPs	GCE	Amperometric	0.5 μM—4.7 mM	60 nM	—	86
	$H_4TCPP/MOF-525$	FTO	Amperometric	20–800 μM	2.1 μM	95 $\mu A\ mM^{-1}$	96
	$MnTMPyP–Ti_4O_9$	GCE	DPV	2.0 μM—1.57 mM	1.25 μM	—	97
Sulphite	CoTRuP/NF	GCE	Cyclic Voltammetry	0–70 mg l^{-1}	7.7 mg l^{-1}		98
	ZnTRuP/FeTPPS	GCE	FIA/Amperometric	8–80 μM	0.5 μM	—	79
	Poly-MTRuP	GCE	Amperometric	1.40–4.68 mg l^{-1}	1.4 mg l^{-1}	—	99
	CoTRuP	GCE	BIA/Amperometric	0.25–500 μM	81 nM	—	76
Bisphenol A	FeTMPP/TRGO membrane	AU	Impidimetric	10^{-12}–10^{-8} M	0.21 pM	—	93
Hydroxilamine	AuNPs/MMPF-6(Fe)	GCE	DPV	0.01–1.0 μM	4 nM	—	100
Ascorbic Acid	TOAB/ERGO@YD	GCE	Amperometric	1.33 μM—1.46 mM	0.28 μM	13.58 $\mu A\ mM^{-1}$	101
	TOAB/YD/MWCNT	GCE	Amperometric	18.72 μM–1.85 mM	0.18 μM	19.16 $\mu A\ mM^{-1}$	102
Glucose	poly[NiTRuP]	GCE	BIA/Amperometric	2.5 μM–1.0 mM	0.36 μM	—	80
Folic Acid	poly[NiTRuP]	GCE	BIA/Amperometric	1–200 μM	0.74 μM	—	103
Catechol	$[(CoTRuP)_n^{8+}]/AuNPs^{n-}$	GCE/ITO	Cyclic Voltammetry	21 μM–1.36 mM	1.4 μM	108 $\mu A\ mM^{-1}$	104
	$\{CoTPyP[Ru(dppb)]_4(\mu Cl_3)_2\}^{4n2+}$	GCE	Cyclic Voltammetry	0.5 μM–1 mM	0.1 μM	—	105
	VOTRuP	GCE	DPV	2–38 μM	0.41 μM	12.73 $\mu A\ mM^{-1}$	85
Hydrogen peroxide	cobalt oxide/CoTRuP	GCE	BIA/Amperometric	0.5 μM—2 mM	0.2 μM	—	106
	Nf/CNT/CoTRuP	GCE	Amperometric	0–1 mM	10.9 μM	8.0 nA mM^{-1}	92
	TOAB/ERGO@ZnPp-C60	GCE	Amperometric	—	0.27 μM	451.3 $\mu A\ mM^{-1}$	107
O_2	CoTRuP/GO	GCE	Amperometric	0–0.66 mM	5.8 μM	—	89
	CoTPP	GCE	Cyclic Voltammetry	62–604 μM	0.4 μM	—	108
Isoniazide	$[CoTRP(dcbpy)_2]$-Ni/GO	GCE	BIA/Amperometric	40–120 μM	3.5 μM	457 μA M	35
Hydroquinone	VOTRuP	GCE	DPV	2–38 μM	0.55 μM	15.91 $\mu A\ mM^{-1}$	85
Acetaminophen	ESP	GCE	Cyclic Voltammetry	0.05–70 mM	5.32 μM	0.04 $\mu A\ mM^{-1}$	109
	CoTRuP-Ba	GCE	SWV	1–50 μM	0.1 μM	0.73 $\mu A\ mM^{-1}$	110
Cd^{2+}	TCPP@ppy	ITO	DPV	0.6–3.4 μM	2.47 $\mu g\ l^{-1}$	19.8 $\mu A\ \mu M^{-1}$	111
Dopamine	$PDP-C_{60}$	GCE	DPV	0–200 μM	0.015 μM	—	112
Tyrosine	CoTRuP-Ba	GCE	SWV	1–24 μM	0.5 μM	0.47 $\mu A\ mM^{-1}$	110
Atrazine	$BMIMNTF_2$/ZnTRuP	GCE	DPV	212–2500	230	—	113
	$BMIMNTF_2$/NiTRuP	GCE	DPV	76.8–3500	540	—	113

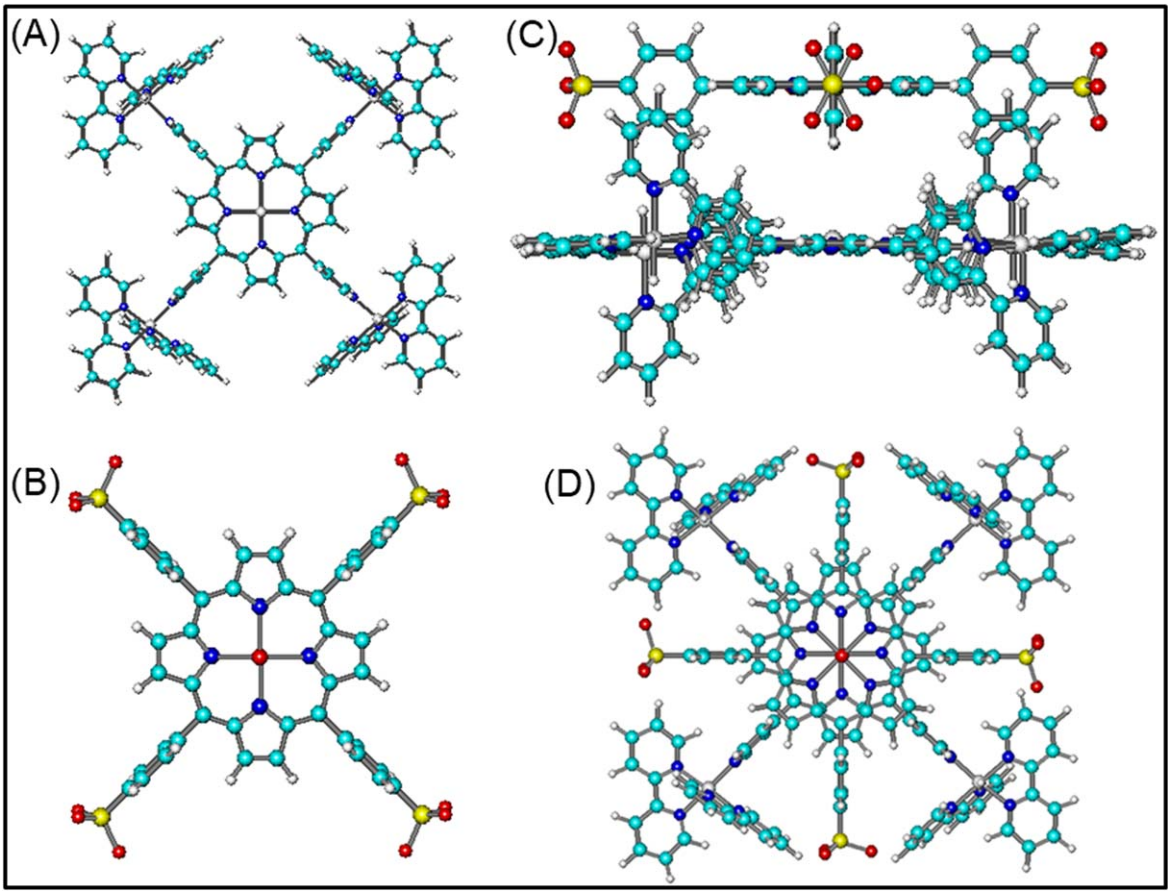

Figure 6. Structure of the (A) cationic porphyrin, (B) anionic porphyrin, and (C) ion-paired porphyrins side view and (D) top view.

is the Ni^{III} porphyrin species electrochemically generated in alkaline medium instead of the Ru^{II}/Ru^{III} centers. A low limit of detection of 0.36 μM was achieved, besides an excellent repeatability (RSD = 1.1% for 25 injections of 25 μM of glucose) by BIA amperometric method.

Recently, Ferreira et al.[81] figured out the mechanism of formation of the poly[NiTRuP] film on the GCE surface by Raman spectroelectrochemistry and Electron Paramagnetic Resonance Spectroscopy (EPR). The formation of poly[NiTRuP] was found to be induced by oxidation of Ru^{II} to Ru^{III} leading to formation of hydroxyl radicals in the 0.8–1.1 V range, responsible for the oxidation of nickel sites to Ni–O–O–Ni bridging species. However, when the potential is superior to 1.1 V oxygen gas bubbles are produced preventing the adherence of the film forming species on the electrode surface. Also, Ferreira et al.[82] electropolymerized mixtures of NiTRuP and CoTRuP in different proportions on the GCE surface in alkaline medium, and obtained excellent electrocatalytic responses for determination of chloramphenicol (antibiotic drug). The cyclic voltammograms of mixed Ni-Co tetraruthenated porphyrins presented only one redox peak indicating the formation of a mixed polymeric NiTRuP/CoTRuP instead of a mixture of two different materials. Also, it was observed that, the redox peak was shifted to less positive potentials while the charge transfer resistance decreased as the proportion of CoTRuP in the film was increased. The electrochemical behavior of those materials were similar to that of $NiCo(OH)_2$.[83,84] However, mixed porphyrin materials containing more than 50% of CoTRuP did not present the typical catalytic response of Ni^{III} species, but showed an increase of current at potentials higher than 0.4 V instead, suggesting the key role of Ni for the catalytic performance of these materials.

Also, Ribeiro et al.[85] determined simultaneously catechol and hydroquinone using an electrode modified with electropolymerized oxovanadium (IV) tetraruthenated porphyrin named VOTRuP. The electropolymerized film was obtained on GCE surface upon successive voltammetric cycling in a 1×10^{-4} mol L^{-1} {VOTPyP[$RuCl_3$(dppb)]} solution in dichloromethane with 0.1 mol L^{-1} tetrabutylammonium hydroxide, in the −0.4 V to +1.0 V *vs* Ag/AgCl range, at scan rate of 100 mV s^{-1}. The electrochemical behavior of bare GCE and electrodes modified with electropolymerized VOTRuP film was verified in the presence of catechol and hydroquinone. The cyclic voltammograms showed an oxidation and reduction peak for catechol and hydroquinone at 575/106 mV (ΔE_p = 469 mV) and 468/111 (ΔE_p = 357 mV) respectively, in the bare GCE. The electrochemical process in the VOTRuP electrode was much more reversible than on bare GCE. In fact, the oxidation and reduction peak of catechol and hydroquinone in the VOTRuP modified electrode were found at 333/303 mV (ΔE_p = 30 mV) and 228/199 mV (ΔE_p = 29 mV), respectively, suggesting that the electropolymerized film is a good redox mediator favoring the heterogeneous electron-transfer from analyte to the electrode. The simultaneous determination of catechol and hydroquinone was performed using differential pulse voltammetry technique where a low LOD and good sensitivity were found for catechol (0.41 μM, 12.73 μA μM) and hydroquinone (0.55 μM, 15.91 μA μM), respectively.

TRuP-based CMEs prepared by periodic assembly method (metal organic frameworks, porous organic polymers and other hybrid materials).—In addition to the modification of electrodes by covalent and noncovalent methods using one or two porphyrins, there are several studies in the literature reporting on the use of CMEs prepared by immobilization of porphyrins in composites and porous organic polymers for sensor application. For example, Muthukumar and Abraham John[86] demonstrated that the metallic

ion coordinated to the porphyrin ring also plays an essential role in the electrocatalysis of substrates such as nitrite. In fact, they reported the electrochemical determination of nitrite using gold nanoparticles (AuNPs) decorated with *meso*-tetra(para-aminophenyl)porphyrinatocobalt(II) (Co(II)MTpAP) self-assembled on GCE surface. The results showed that the Co(II)MTpAP/cit-AuNPs nanoconjugate not only shifts the nitrite oxidation potential to less positive potentials but also increased the respective anodic current as compared with pure Co(II)MTpAP, where the limit of detection was 60 nM by an amperometric method. In order to understand the role of central metal ion in the oxidation mechanism of nitrite, a linear sweep voltammetry was performed using an electrode based on Co(II) MTpAP/cit-AuNPs and another electrode modified with the free-base derivative of that porphyrin material, MTpAP/cit-AuNPs, in the presence of nitrite ion. The substrate oxidation occurred at the same potential for both electrodes but the anodic current intensity was much higher for the electrode based on the metallated derivative, thus demonstrating the significant role of that metal ion on the conductivity and electron transport efficiency of the material via tunneling mechanism.[87]

Also, carbon materials such as graphene, fullerene and carbon nanotubes have been employed in electrochemical sensors due to their excellent conductivity and electron-transfer kinetics. In this sense, Jahan et al.[88] developed an electrode based on graphene and metalloporphyrins immobilized by formation of a Metal-Organic Framework (MOF), where the electrode was obtained by reacting pyridine-functionalized graphene with the iron-porphyrin in order to enhance its catalytic activity for oxygen reduction reaction. It was observed that the electrochemical charge-transfer rate of iron-porphyrin was improved by crystallization of the iron-porphyrin in the MOF caused by addition of pyridine-functionalized graphene.

Similarly, Saravia et al.[89] modified an electrode by drop casting the CoTRuP/GO composite, prepared upon immobilization of CoTRuP on graphene oxide (GO) by mixing its aqueous solution with a GO dispersion in different proportion. Spectroscopic studies showed that CoTRuP is strongly supported on GO by electrostatic interactions, but there was an optimal proportion of CoTRuP and GO that maximized the electrocatalytic activity of the composite material for oxygen reduction reaction. Indeed, the best performance was obtained when the proportion of CoTRuP:GO is 1:4. larger proportions of GO lead to aggregation induced by π-π interactions between GO sheets, hindering access to the electrocatalytic sites of cobalt porphyrin, thus decreasing the catalytic performance of the nanocomposite.[90] In addition, the CoTRuP/GO nanocomposite presented a good limit of detection of 5.8 μM for O_2 dissolved in aqueous medium.

Another carbon material largely used as heterogeneous catalyst support in electrochemical sensor construction are the multi-walled carbon nanotubes (MWCNTs), because of their favorable electronic, mechanical, and conductivity properties.[91] Calfumán et al.[92] incorporated carbon nanotubes to electrodes modified with Nafion/CoTRuP in order to determine hydrogen peroxide. Electrochemical Scanning Microscopy studies were performed in order to understand the topography and the electrochemical activity of Nf/CoTRuP, Nf/CNT/CoTRuP, and Nf/CNT modified electrodes, in the presence of Ferrocenemethanol (FcOH). The tip potential was set to 0.6 V *vs* Ag/AgCl, high enough to oxidize FcOH while the substrate was maintained at −0.1 V *vs* Ag/AgCl to regenerate the electron-transfer mediator and provide a feedback current between the tip and the substrate. The Nf/CNT electrode presented regions with different electrochemical activity, indicating areas with different amounts of CNT. In contrast, the Nf/CoTRuP and Nf/CNT/CoTRuP electrodes exhibited a comparatively more homogeneous surface. In addition, the Nf/CNT/CoTRuP electrode presented a much higher roughness than that expected for the presence of CNT, consistent with its higher catalytic activity. A limit of detection of 10.9 μA and a sensitivity of 8.0 nA μM were achieved employing the Nf/CNT/CoTRuP electrode as electrochemical hydrogen peroxide sensor, using an amperometric method.

It is also important to note that low limits of detection can be achieved using other electrochemical techniques such as impedimetric instead of voltammetric or amperometric methods. In fact, Hsine et al.[93] prepared electrodes modified with an iron(III) porphyrin (Fe(III)TMPP) and thermally reduced graphene oxide (TRGO), TRGO/Fe(III)TMPP. This CME was used as impedimetric sensor for Bisphenol A that achieved a very low limit of detection of 0.21 pM. The modified electrode was prepared by drop-casting TRGO on Au electrode surface and drying at 80 °C in an oven for 1 h. Then, a porphyrin solution was drop-casted onto the TRGO/Au and dried at room temperature.

The red shift of the porphyrin Soret and Q bands suggested strong π-π interactions between the delocalized TRGO and porphyrin π-systems,[94] that was confirmed by Electrochemical Impedance Spectroscopy (EIS) based on a systematic study using Au, Au/TRGO, Au/Fe(III)TMPP and Au/Fe(III)TMPP/TRGO. The R_{ct} decreased from the Au electrode (15.23 kΩ) to Au/TRGO (8.34 kΩ) showing that TRGO improved the charge-transfer of Au electrodes. The R_{ct} of Au/Fe(III)TMPP was slightly higher (10.10 kΩ) but decreased to 4.11 kΩ when TRGO was added confirming the enhanced charge-transfer and good π-stacking interaction of TRGO and Fe(III)TMPP.

Then, the CME was tested as impedimetric sensor in the presence of increasing concentrations of Bisphenol A, in the frequency range from 100 kHz to 30 mHz, with a polarization potential of −0.9 V. Two semi-circles were observed in the Nyquist plot, as well as an increase of R_{ct} as a function of concentration of Bisphenol A, that was assigned to its adsorption on the nanocomposite multilayers, thus changing the electrochemical properties of the interface.

Highly hierarchical structures (two-dimensional or three-dimensional) with new functions and applications such as molecular recognition, sensing and catalysis can be realized by coordination-driven assemblies. In this context, porphyrins and metalloporphyrins have proven to be excellent building blocks for the development of two and three-dimensional materials such as MOFs.[13] In fact, this immobilization strategy was used by Aguirre-Araque et al.[35] to prepare a new coordination polymer based on a CoTPyP coordinated to four $[Ru(H_2dcbpy)_2Cl]^+$ moieties. The tetraruthenated porphyrin was first deposited onto GO sheets and a coordination polymer was then formed in the presence of an excess of nickel(II) ions, that act as bridge through the carboxylate groups of the peripheral ruthenium complexes. This polymeric neutral or less negatively charged species can interact much better with the negatively charged GO sheets, generating the composite named as [CoTRuP(dcbpy)$_2$]-Ni/GO. The formation of a lamellar structure was confirmed by XRD, where the (001) reflection plane of GO was shifted from 2θ 11.3° to 6.5° in the composite, evidencing the formation of a lamellar material with [CoTRuP(dcbpy)$_2$]-Ni intercalated in between GO sheets. Then, a new electrochemical sensor for isoniazide was prepared by immobilization of [CoTRuP(dcbpy)$_2$]-Ni/GO on GC electrodes. The measurements carried out by BIA/amperometric technique using a working potential of 0.1 V *vs* Ag/AgCl and pH 7 indicated a sensitivity of 457 μA M^{-1} and a limit of detection of 3.53 μM.

GCE = glassy carbon electrode, FIA = flow injection analysis, CoTMPyP = 5, 10,15, 20-tetrakis (N-methylpyridinium-4-yl) porphyrinato cobalt(III), DPV = differential pulse voltammetry, Co(II) MTpAP = meso-tetra(para-aminophenyl)porphyrinat cobalt(II), cit-AuNPs = citrate-gold nanoparticles, H4TCPP = meso-tetra(4-carboxyphenyl)porphyrin, MOF-525 = hexa-zirconium nodes, FTO = fluorine doped tin oxide, MnTMPyP = 5,10,15,20-tetrakis (N-methylpyridinium-4-yl) porphyrinato manganese(III), NF = nafion, Poly-MTRuP = polymerized metallated tetraruthenated porphyrin, where M = Ni(II) and Zn(II)), BIA = Batch Injection Analysis, FeTMPP = 5,10,15,20-tetrakis(4-metoxyphenyl) porphyrinato iron(III), TRGO = thermally reduced graphene oxide, Au = gold electrode, MMPF-6(Fe) = metal−metalloporphyrin frameworks, TOAB = tetraoctylammonium bromide, ERGO = electrochemically reduced graphene oxide, YD = 5,15-bis(2,6-

dioctoxyphenyl)−10-(bis(4-hexylphenyl)amino-20,4-carboxyphenyl ethynyl)porphyrinato zinc (II), MWCNT = multi-walled carbon nanotubes, Gr = Graphene, CoTPP = 5, 10, 15, 20-meso-tetraphenylporphyrinato cobalt (II)), [CoTRuP(dcbpy)$_2$]-Ni = tetrapyridylporphyrinato cobalt(III) (CoTPyP) coordinated to four [Ru(dcbpy)$_2$Cl] complexes, VOTRuP = tetraruthenated oxovanadium(IV) porphyrin, ESP = electropolymerized supramolecular porphyrins Mn-TPyP(H$_2$O)$_2$[RuCl$_3$(dppb)]$_4$}PF$_6$, Ba = Cameroonian smectite clay (from Bagba hill, denoted Ba), SWV = Square Wave Voltammetry, TCPP = meso-(tetracarboxyphenyl) porphyrin, ppy = polypyrrole, PDP = porphyrin-diazocine-porphyrin, C_{60} = fullerene. BMIMNTF$_2$ = 1-butyl-3-methylimidazolium bis (trifluoromethylsulfonyl) imide.

Summary and Outlook

In the field of electro and photoelectrocatalysts, TRuPs modified electrodes have been reported as excellent catalysts for CO_2 reduction to produce useful chemicals such as methane, methanol, ethanol, formaldehyde and formic acid. Enhanced catalytic activity was demonstrated using Nafion (Nf) and polyvinyl chloride (PVC) as a polymeric support to immobilize the MTRuPs (electrodes modified with MTRuP/PVP or MTRuP/Nf). In fact, it was shown by electrochemical impedance spectroscopy that PVC electrodes present a non-uniform surface resulting in higher capacitances that compensate the slow electrochemical reactions. These were associated with three different relaxation times, consistent with three different charge storage sites or, in other words, three active sites for reaction that explain the high TOF values obtained for the GC/PVC/MTRuP and GC/Nf/MTRuP modified electrodes.

Analogous behavior was also observed when GC/PVC/MTRuP and GC/Nf/MTRuP modified electrodes were applied as catalysts for NO_2^- reduction, where the effect of metal ions in MTRuP was assessed. The macrocycle ring itself is the catalytic site for reduction of nitrite when a closed shell transition metal ion such as Zn^{2+} is coordinated to the porphyrin.[60,114] In contrast, the metal ion in CoTRuP is electrochemically active and can be oxidized activating the catalyst while providing an interaction site for nitrite, as confirmed by the shift of the Soret band,[65] and a more stable catalyst than the one based on the π-radical cation.[60]

Additionally, the electrocatalytic properties of porphyrin materials have been transferred to electrodes enhancing the sensitivity for detection of many analytes such as nitrite, sulfite, ascorbic acid, glucose, and hydrogen peroxide among others. Accordingly, methods such as covalent, noncovalent and periodic assembly methods, for example, anchoring by dip-coating, drop-casting, layer-by-layer, electropolymerization or by formation of metal organic frameworks and other hybrid materials have been reported to immobilize them onto electrode surface. Among them, the ion-pairing strategy of cationic and anionic porphyrins (noncovalent method) was proven to be a very interesting to avoid leaching/solubilization of porphyrin materials. Also, the use of carbon materials such as GO, RGO, carbon nanotubes, and fullerenes in association with porphyrins, has proven to be an excellent strategy for obtaining more conductive and electrochemically active materials. Finally, the choice of the detection method was shown to be as important as the electrochemical sensor. In fact, techniques such as electrochemical impedance are more suitable when it comes to obtaining higher sensitivities. In short, the exceptional electrocatalytic and photochemical properties of porphyrins are being exploited for preparation of new hybrid, composite and higher order hierarchical materials such as 2D and 3D coordination polymers and MOFs, opening new perspectives on the use of transition metal complexes to assemble structures beyond tetraruthenated porphyrins, and explore new applications such as the production of valuable chemicals and solar fuels.

Acknowledgments

This work was supported by the Sao Paulo Research Foundation (FAPESP processes 2018/21489-1, 2017/13137-5, 2017/50129-0 and 2013/24725-4) and the National Council for Scientific and Technological Development (CNPq 442599/2019-6, 303137/2016-9, 401581/2016-0, 408222/2016-6), INCT/FAPESP (Process 2014/50867-3), CAPES/STINT-PROJ-20191341444P in addition to the fellowships granted to J.M.G. (FAPESP 2018/16896-7).

ORCID

Josué M. Gonçalves https://orcid.org/0000-0003-0800-077X
Koiti Araki https://orcid.org/0000-0003-3485-4592

References

1. H. E. Toma and K. Araki, *Coord. Chem. Rev.*, **196**, 307 (2000).
2. J.-M. Lehn, *Angew. Chem. Int. Ed. Engl.*, **27**, 89 (1988).
3. T. A. Matias, G. C. Azzellini, L. Angnes, and K. Araki, *Electrochemistry of N4 Macrocyclic Metal Complexes: Biomimesis, Electroanalysis and Electrosynthesis of MN4 Metal Complexes*, ed. J. H. Zagal and F. Bedioui (Springer International Publishing, Cham) Vol. 2, p. 1 (2016).
4. S. Lesage, H. A. O. Xu, and L. Durham, *Hydrol. Sci. J.*, **38**, 343 (1993).
5. K. Kadish, K. M. Smith, and R. Guilard, *The Porphyrin Handbook* (Elsevier, Amsterdam) (2000).
6. G. M. Mason, L. G. Trudell, and J. F. Branthaver, *Org. Geochem.*, **14**, 585 (1989).
7. P. Rothemund, *JACS*, **57**, 2010 (1935).
8. H. Shy, P. Mackin, A. S. Orvieto, D. Gharbharan, G. R. Peterson, N. Bampos, and T. D. Hamilton, *Faraday Discuss.*, **170**, 59 (2014).
9. R. De Paula, M. A. F. Faustino, D. C. G. A. Pinto, M. G. P. M. S. Neves, and J. A. S. Cavaleiro, *J. Heterocycl. Chem.*, **45**, 453 (2008).
10. T. D. Lash, *Chemistry—A European Journal*, **2**, 1197 (1996).
11. G. C. Ferreira, K. M. Kadish, K. M. Smith, and R. Guilard, *The Handbook of Porphyrin Science* (World Scientific, Singapore) (2013).
12. E. Prigorchenko, L. Ustrnul, V. Borovkov, and R. Aav, *J. Porphyrins Phthalocyanines*, **23**, 1308 (2019).
13. E. G. Percástegui and V. Jancik, *Coord. Chem. Rev.*, **407**, 213165 (2020).
14. A. D. Adler, F. R. Longo, J. D. Finarelli, J. Goldmacher, J. Assour, and L. Korsakoff, *The Journal of Organic Chemistry*, **32**, 476 (1967).
15. J. S. Lindsey, I. C. Schreiman, H. C. Hsu, P. C. Kearney, and A. M. Marguerettaz, *The Journal of Organic Chemistry*, **52**, 827 (1987).
16. K. Araki and H. E. Toma, *J. Coord. Chem.*, **30**, 9 (1993).
17. K. Araki and H. E. Toma, *J. Photochem. Photobiol., A*, **83**, 245 (1994).
18. H. Winnischofer, S. de Souza Lima, K. Araki, and H. E. Toma, *Anal. Chim. Acta*, **480**, 97 (2003).
19. S. Dovidauskas, K. Araki, and H. E. Toma, *J. Porphyrins Phthalocyanines*, **4**, 727 (2000).
20. L. L. Romualdo, A. L. Bogado, E. M. A. Valle, I. S. Moreira, J. Ellena, E. E. Castellano, M. P. de Araujo, and A. A. Batista, *Polyhedron*, **27**, 53 (2008).
21. I. Mayer, A. L. B. Formiga, F. M. Engelmann, H. Winnischofer, P. V. Oliveira, D. M. Tomazela, M. N. Eberlin, H. E. Toma, and K. Araki, *Inorg. Chim. Acta*, **358**, 2629 (2005).
22. A. L. B. Formiga, A. F. Nogueira, K. Araki, and H. E. Toma, *New J. Chem.*, **32**, 1167 (2008).
23. J. A. Bonacin, V. Katic, K. C. F. Toledo, and H. E. Toma, *Inorg. Chim. Acta*, **437**, 127 (2015).
24. I. Mayer, M. N. Eberlin, D. M. Tomazela, H. E. Toma, and K. Araki, *J. Braz. Chem. Soc.*, **16**, 418 (2005).
25. K. Araki, L. Angnes, and H. E. Toma, *Adv. Mater.*, **7**, 554 (1995).
26. K. Araki, L. Angnes, C. M. N. Azevedo, and H. E. Toma, *J. Electroanal. Chem.*, **397**, 205 (1995).
27. K. Araki and H. E. Toma, *Electrochim. Acta*, **44**, 1577 (1999).
28. O. A. C. Viviane Viecelli, K. Araki, P. R. Martins, and B. A. Iglesias, *J. Braz. Chem. Soc.* (2020).
29. K. Araki, S. Dovidauskas, H. Winnischofer, A. D. P. Alexiou, and H. E. Toma, *J. Electroanal. Chem.*, **498**, 152 (2001).
30. S. Dovidauskas, H. E. Toma, K. Araki, H. C. Sacco, and Y. Iamamoto, *Inorg. Chim. Acta*, **305**, 206 (2000).
31. M. I. F. Barbosa et al., *J. Photochem. Photobiol., A*, **338**, 152 (2017).
32. R. N. Sampaio, M. M. Silva, A. A. Batista, and N. M. B. Neto, *J. Photochem. Photobiol., A*, **315**, 98 (2016).
33. M. Gouterman, *J. Mol. Spectrosc.*, **6**, 138 (1961).
34. L. P. H. Saravia, A. Sukeri, J. M. Gonçalves, J. S. Aguirre-Araque, B. B. N. S. Brandão, T. A. Matias, M. Nakamura, K. Araki, H. E. Toma, and M. Bertotti, *Electrochim. Acta*, **222**, 1682 (2016).
35. J. S. Aguirre-Araque, J. M. Gonçalves, M. Nakamura, P. O. Rossini, L. Angnes, K. Araki, and H. E. Toma, *Electrochim. Acta*, **300**, 113 (2019).
36. T. H. O. Leite et al., *Inorg. Chem.*, **58**, 1030 (2019).
37. L. Sun, V. Reddu, A. C. Fisher, and X. Wang, *Energ Environ Sci*, **13**, 374 (2020).
38. M. d. F. B. Souza, *Química Nova*, **20**, 191 (1997).
39. I. K. Attatsi, W. Zhu, and X. Liang, *New J. Chem.*, **44**, 4340 (2020).
40. X.-M. Hu, Z. Salmi, M. Lillethorup, E. B. Pedersen, M. Robert, S. U. Pedersen, T. Skrydstrup, and K. Daasbjerg, *Chem. Commun.*, **52**, 5864 (2016).

41. Y. Xiao, W. Guo, H. Chen, H. Li, X. Xu, P. Wu, Y. Shen, B. Zheng, F. Huo, and W. D. Wei, *Mater. Chem. Front.*, **3**, 1580 (2019).
42. P. T. Smith, B. P. Benke, Z. Cao, Y. Kim, E. M. Nichols, K. Kim, and C. J. Chang, *Angew. Chem. Int. Ed.*, **57**, 9684 (2018).
43. N. Han et al., *Chem*, **3**, 652 (2017).
44. X.-D. Zhang, S.-Z. Hou, J.-X. Wu, and Z.-Y. Gu, *Chemistry—A European Journal*, **26**, 1604 (2020).
45. K. Elouarzaki, V. Kannan, V. Jose, H. S. Sabharwal, and J.-M. Lee, *Adv. Energy Mater.*, **9**, 1900090 (2019).
46. P. Gotico, Z. Halime, and A. Aukauloo, *Dalton T*, **49**, 2381 (2020).
47. X.-M. Hu, S. U. Pedersen, and K. Daasbjerg, *Current Opinion in Electrochemistry*, **15**, 148 (2019).
48. N. Corbin, J. Zeng, K. Williams, and K. Manthiram, *Nano Res.*, **12**, 2093 (2019).
49. C. Jiang, A. W. Nichols, and C. W. Machan, *Dalton T*, **48**, 9454 (2019).
50. I. Mayer, G. S. Nunes, H. E. Toma, and K. Araki, *Eur. J. Inorg. Chem.*, **2006**, 850 (2006).
51. G. S. Nunes, I. Mayer, H. E. Toma, and K. Araki, *J. Catal.*, **236**, 55 (2005).
52. H.-Z. Yu, J. S. Baskin, B. Steiger, F. C. Anson, and A. H. Zewail, *JACS*, **121**, 484 (1999).
53. F. C. Anson, C. Shi, and B. Steiger, *Acc. Chem. Res.*, **30**, 437 (1997).
54. C. Shi and F. C. Anson, *Inorg. Chem.*, **31**, 5078 (1992).
55. A. N. Oldacre, A. E. Friedman, and T. R. Cook, *JACS*, **139**, 1424 (2017).
56. A. N. Oldacre, M. R. Crawley, A. E. Friedman, and T. R. Cook, *Chemistry—A European Journal*, **24**, 10984 (2018).
57. M. García, M. J. Aguirre, G. Canzi, C. P. Kubiak, M. Ohlbaum, and M. Isaacs, *Electrochim. Acta*, **115**, 146 (2014).
58. M. García, K. Carfumán, C. Díaz, C. Garrido, I. Osorio-Román, M. J. Aguirre, and M. Isaacs, *Electrochim. Acta*, **80**, 390 (2012).
59. K. Calfumán, J. Honores, D. Guzmán, M. Ohlbaum, F. Armijo, R. Del Río, and M. Isaacs, *Chemelectrochem*, **4**, 3314 (2017).
60. K. Calfumán, P. Dreyse, C. García, M. J. Aguirre, T. Beltrán, E. Guillamón, I. Sorribes, C. Vicent, R. Llusar, and M. Isaacs, *Macromolecular Symposia*, **304**, 93 (2011).
61. A. Kumar, J. M. Gonçalves, A. Sukeri, K. Araki, and M. Bertotti, *Sensors Actuators B*, **263**, 237 (2018).
62. A. M. Fan and V. E. Steinberg, *Regul. Toxicol. Pharm.*, **23**, 35 (1996).
63. T. P. Xie, Y. F. Zhao, L. Q. Chen, Z. J. Zhu, Y. Hu, and Y. Yuan, *Diseases of the Esophagus*, **24**, 30 (2011).
64. J. Zhao, X. Wang, Z. Xu, and J. S. C. Loo, *J Mater Chem A*, **2**, 15228 (2014).
65. K. Calfumán, M. J. Aguirre, P. Cañete-Rosales, S. Bollo, R. Llusar, and M. Isaacs, *Electrochim. Acta*, **56**, 8484 (2011).
66. F. Roncaroli and R. van Eldik, *JACS*, **128**, 8042 (2006).
67. M. García et al., *Electrochim. Acta*, **192**, 61 (2016).
68. P. A. Dreyse, M. A. Isaacs, P. E. Iturriaga, D. A. Villagra, M. J. Aguirre, C. P. Kubiak, S. D. Glover, and J. C. Goeltz, *J. Electroanal. Chem.*, **648**, 98 (2010).
69. P. Dreyse, M. Isaacs, K. Calfumán, C. Cáceres, A. Aliaga, M. J. Aguirre, and D. Villagra, *Electrochim. Acta*, **56**, 5230 (2011).
70. I. Mayer, H. E. Toma, and K. Araki, *J. Electroanal. Chem.*, **590**, 111 (2006).
71. M. Isaacs, F. Armijo, G. Ramírez, E. Trollund, S. R. Biaggio, J. Costamagna, and M. J. Aguirre, *J. Mol. Catal. A: Chem.*, **229**, 249 (2005).
72. J. Costamagna, M. Isaacs, M. J. Aguirre, G. Ramirez, and I. Azocar, "Electroreduction of CO2 Catalyzed by Metallomacrocyclics." *N4-Macrocyclic Metal Complexes*, ed. J. H. Zagal, F. Bedioui, and J-P. Dodelet (Springer, New York, NY)191 (2006).
73. W.-L. He, J.-L. Chen, M. Chen, and D.-J. Qian, *Colloids Surf., A*, **509**, 1 (2016).
74. L. Angnes, C. M. N. Azevedo, K. Araki, and H. E. Toma, *Anal. Chim. Acta*, **329**, 91 (1996).
75. M. S. M. Quintino, K. Araki, H. E. Toma, and L. Angnes, *Electroanalysis*, **14**, 1629 (2002).
76. M. S. M. Quintino, K. Araki, H. E. Toma, and L. Angnes, *Talanta*, **68**, 1281 (2006).
77. K. Araki, M. J. Wagner, and M. S. Wrighton, *Langmuir*, **12**, 5393 (1996).
78. J. R. C. da Rocha, L. Angnes, M. Bertotti, K. Araki, and H. E. Toma, *Anal. Chim. Acta*, **452**, 23 (2002).
79. P. R. Martins, W. D. Popolim, L. A. F. Nagato, E. Takemoto, K. Araki, H. E. Toma, L. Angnes, and M. D. V. C. Penteado, *Food Chem.*, **127**, 249 (2011).
80. M. d. S. M. Quintino, H. Winnischofer, M. Nakamura, K. Araki, H. E. Toma, and L. Angnes, *Anal. Chim. Acta*, **539**, 215 (2005).
81. L. M. C. Ferreira, D. Grasseschi, M. S. F. Santos, P. R. Martins, I. G. R. Gutz, A. M. C. Ferreira, K. Araki, H. E. Toma, and L. Angnes, *Langmuir*, **31**, 4351 (2015).
82. L. M. C. Ferreira, P. R. Martins, K. Araki, and L. Angnes, *Electroanalysis*, **31**, 688 (2019).
83. P. R. Martins, A. L. Araújo Parussulo, S. H. Toma, M. A. Rocha, H. E. Toma, and K. Araki, *J. Power Sources*, **218**, 1 (2012).
84. P. R. Martins, L. M. C. Ferreira, K. Araki, and L. Angnes, *Sensors Actuators B*, **192**, 601 (2014).
85. G. H. Ribeiro, L. M. Vilarinho, T. D. S. Ramos, A. L. Bogado, and L. R. Dinelli, *Electrochim. Acta*, **176**, 394 (2015).
86. P. Muthukumar and S. Abraham John, *J. Colloid Interface Sci.*, **421**, 78 (2014).
87. X. Lu, M. Li, C. Yang, L. Zhang, Y. Li, L. Jiang, H. Li, L. Jiang, C. Liu, and W. Hu, *Langmuir*, **22**, 3035 (2006).
88. M. Jahan, Q. Bao, and K. P. Loh, *JACS*, **134**, 6707 (2012).
89. L. P. H. Saravia, A. Sukeri, J. M. Gonçalves, J. S. Aguirre-Araque, B. B. N. S. Brandão, T. A. Matias, M. Nakamura, K. Araki, H. E. Toma, and M. Bertotti, *Electrochim. Acta*, **222**, 1682 (2016).
90. P. Fisicaro, A. Adriaens, E. Ferrara, and E. Prenesti, *Anal. Chim. Acta*, **597**, 75 (2007).
91. C. B. Jacobs, M. J. Peairs, and B. J. Venton, *Anal. Chim. Acta*, **662**, 105 (2010).
92. K. Calfumán, D. Quezada, M. Isaacs, and S. Bollo, *Electroanalysis*, **27**, 2778 (2015).
93. Z. Hsine, S. Bizid, I. Zahou, L. Ben Haj Hassen, H. Nasri, and R. Mlika, *Synth. Met.*, **244**, 27 (2018).
94. C. Socaci, F. Pogacean, A. R. Biris, M. Coros, M. C. Rosu, L. Magerusan, G. Katona, and S. Pruneanu, *Talanta*, **148**, 511 (2016).
95. Z. Fan, Z. Ding, X. Zhang, S. Wu, M. Wang, and Z. Tong, *Mater. Lett.*, **253**, 281 (2019).
96. C.-W. Kung, T.-H. Chang, L.-Y. Chou, J. T. Hupp, O. K. Farha, and K.-C. Ho, *Electrochem. Commun.*, **58**, 51 (2015).
97. J. Ma, M. Yang, Y. Chen, L. Liu, X. Zhang, M. Wang, D. Zhang, and Z. Tong, *Mater. Lett.*, **150**, 122 (2015).
98. K. Calfumán, M. J. Aguirre, D. Villagra, C. Yañez, C. Arévalo, B. Matsuhiro, L. Mendoza, and M. Isaacs, *J. Solid State Electrochem.*, **14**, 1065 (2010).
99. P. Dreyse, D. Quezada, J. Honores, M. J. Aguirre, L. Mendoza, B. Matsuhiro, D. Villagra, and M. Isaacs, *Electroanalysis*, **24**, 1709 (2012).
100. Y. Wang, L. Wang, H. Chen, X. Hu, and S. Ma, *ACS Applied Materials & Interfaces*, **8**, 18173 (2016).
101. H. Wu, X. Li, M. Chen, C. Wang, T. Wei, H. Zhang, and S. Fan, *Electrochim. Acta*, **259**, 355 (2018).
102. D. Huang, X. Li, M. Chen, F. Chen, Z. Wan, R. Rui, R. Wang, S. Fan, and H. Wu, *J. Electroanal. Chem.*, **841**, 101 (2019).
103. L. M. C. Ferreira, P. R. Martins, K. Araki, H. H. Toma, and L. Angnes, *Electroanal*, **27**, 2322 (2015).
104. L. M. Sousa, L. M. Vilarinho, G. H. Ribeiro, A. L. Bogado, and L. R. Dinelli, *Royal Society Open Science*, **4**, 11 (2017).
105. L. R. Dinelli, G. Von Poelhsitz, E. E. Castellano, J. Ellena, S. E. Galembeck, and A. A. Batista, *Inorg. Chem.*, **48**, 4692 (2009).
106. M. S. M. Quintino, H. Winnischofer, K. Araki, H. E. Toma, and L. Angnes, *Analyst*, **130**, 221 (2005).
107. S. Fan, J. yang, T. Wei, J. Zhang, N. Zhang, M. Chai, X. Jin, and H. Wu, *Talanta*, **160**, 713 (2016).
108. L. P. H. Saravia, S. Anandhakumar, A. L. A. Parussulo, T. A. Matias, C. C. Caldeira da Silva, A. J. Kowaltowski, K. Araki, and M. Bertotti, *J. Electroanal. Chem.*, **775**, 72 (2016).
109. M. M. d. Silva, G. H. Ribeiro, A. A. Batista, A. M. d. Faria, A. L. Bogado, and L. R. Dinelli, *J. Braz. Chem. Soc.*, **24**, 1772 (2013).
110. J. C. Kemmegne-Mbouguen, H. E. Toma, K. Araki, V. R. L. Constantino, E. Ngameni, and L. Angnes, *Microchim. Acta*, **183**, 3243 (2016).
111. S. Peshoria and A. K. Narula, *Materials Science and Engineering: B*, **229**, 53 (2018).
112. M. Zhang and J. Li, *Dyes Pigm.*, **173**, 107966 (2020).
113. K. Calfumán, J. Honores, M. Isaacs, D. Quezada, J. Valdebenito, and M. Urzúa, *Electroanal*, **31**, 671 (2019).
114. J. Zhang, F. Zhao, and M. Kaneko, *J. Porphyrins Phthalocyanines*, **4**, 65 (2000).